

Review

# State-of-the-Art Developments in Advanced Hard Ceramic Coatings Using PVD Techniques for High-Temperature Tribological Applications

Dinesh Kumar Devarajan <sup>1,2,\*</sup> , Baskaran Rangasamy <sup>3</sup>  and Kamalan Kirubakaran Amirtharaj Mosas <sup>4,\*</sup> 

<sup>1</sup> Centre for Nanoscience and Nanotechnology, Sathyabama Institute of Science and Technology, Jeppiaar Nagar 600119, Tamil Nadu, India

<sup>2</sup> Sathyabama Centre for Advanced Studies, Sathyabama Institute of Science and Technology, Jeppiaar Nagar 600119, Tamil Nadu, India

<sup>3</sup> Energy Storage Materials and Devices Lab, Department of Physics, School of Mathematics and Natural Sciences, The Copperbelt University, Riverside, Jambo Drive, P.O. Box 21692, Kitwe 10101, Zambia

<sup>4</sup> Coating Department, FunGlass, Centre for Functional and Surface Functionalized Glass, Alexander Dubcek University of Trencin, 91150 Trencin, Slovakia

\* Correspondence: ddinesh.tribology@gmail.com (D.K.D.); kamalan.mosas@tuni.sk (K.K.A.M.)

**Abstract:** Hard and wear-resistant coatings created utilizing physical vapor deposition (PVD) techniques are extensively used in extreme tribological applications. The friction and wear behavior of coatings vary significantly with temperature, indicating that advanced coating concepts are essential for prolonged load-bearing applications. Many coating concepts have recently been explored in this area, including multicomponent, multilayer, gradient coatings; high entropy alloy (HEA) nitride; and functionally modified coatings. In this review, we highlighted the most significant findings from ongoing research to comprehend crucial coating properties and design aspects. To obtain enhanced tribological properties, the microstructure, composition, residual stress, hardness, and HT oxidation resistance are tuned through doping or addition of appropriate materials at an optimized level into the primary coatings. Such improvements are achieved by optimizing PVD process parameters such as input power, partial pressure, reactive gas flow rates, substrate bias, and temperature. The incorporation of ideal amounts of Si, Cr, Mo, W, Ag, and Cu into ternary and quaternary coatings, as well as unique multilayer designs, considerably increases the tribological performance of the coatings. Recent discoveries show that not only mechanical hardness and fracture toughness govern wear resistance, but also that oxidation at HT plays a significant role in the lubrication or wear failure of coatings. The tribo-induced metal oxides and/or Magnéli phases concentrated in the tribolayer are the key governing factors of friction and wear behavior at high temperatures. This review includes detailed insights into the advancements in wear resistance as well as various failure mechanisms associated with temperature changes.

**Keywords:** hard coatings; high temperature; HiPIMS; wear resistance; oxidation; tribolayer



**Citation:** Devarajan, D.K.; Rangasamy, B.; Amirtharaj Mosas, K.K. State-of-the-Art Developments in Advanced Hard Ceramic Coatings Using PVD Techniques for High-Temperature Tribological Applications. *Ceramics* **2023**, *6*, 301–329. <https://doi.org/10.3390/ceramics6010019>

Academic Editor: Angel L. Ortiz

Received: 23 December 2022

Revised: 9 January 2023

Accepted: 17 January 2023

Published: 21 January 2023



**Copyright:** © 2023 by the authors. Licensee MDPI, Basel, Switzerland. This article is an open access article distributed under the terms and conditions of the Creative Commons Attribution (CC BY) license (<https://creativecommons.org/licenses/by/4.0/>).

## 1. Introduction and Need for Hard Coatings

Hard, protective coatings on moving mechanical assemblies are essential in modern industries to protect components operated under high-temperature (HT) and harsh environments to extend their lifetime and reduce wear-/corrosion-related losses. Tribological, hard coatings include metals, nitrides, carbides, oxides, and borides of transition metals [1,2]. Nitride-based hard coatings are frequently used as protective coating materials to protect from wear and corrosion and to extend the prolonged sustainability of high-speed cutting tools, aerospace components, and gas turbines owing to their superior properties, such as high hardness, corrosion resistance, high-temperature stability, low friction, and wear resistance [3,4]. More specifically, recent developments in Al-incorporated transition

metal nitride (TMN) coatings have already demonstrated their role in the enhancement of mechanical and HT tribological properties. The thermal stability of TMN coatings is greatly influenced by the defect structure, interdiffusion, grain refinement, and solid solutions. These phenomena are scientifically significant since the resulting structure has a large impact on the mechanical and tribological properties of the coating [5]. Therefore, the development of advanced hard ceramic coatings can be achieved by tailoring the coating structure of single-layer coatings by adding suitable elements and fabricating novel coating architectures, such as multilayer and multicomponent nanocomposite coatings. Many key findings have indicated that tuning the microstructure of hard coatings has a considerable effect on friction and wear resistance properties [6–8]. Sabzi et al. [8] observed a significant reduction in friction (0.08) and wear for a Ni-W<sub>2</sub>C (20 wt% W<sub>2</sub>C) nanocomposite coating compared to a Ni coating (CoF: 0.72), owing to the dendritic microstructure with a uniform distribution of W<sub>2</sub>C nanoparticles.

Generally, tribological coatings are classified into three major categories: soft coatings with hardness less than 10 GPa, hard coatings with hardness greater than 10 GPa, and superhard coatings with hardness greater than 40 GPa [9,10]. Ceramic coatings such as aluminum oxide, titanium nitride (TiN), and titanium carbide (TiC) have successfully been applied to cutting tools, providing enhanced protection against abrasive and diffusion wear at high temperatures, resulting in a more than ten-fold increase in lifetime. Ceramic coatings have higher mechanical properties than metal coatings because of the solid solution strengthening caused by gas atoms that create point defects in the metallic crystal lattice, preventing dislocation motion [11].

Ternary hard coatings, TiAlN and CrAlN, are commercially employed in a wide range of industrial applications due to their exceptional physical and chemical properties, which include high hardness, fracture toughness, and chemical stability [12]. Many studies have been conducted to overcome the higher friction behavior of these coatings by designing unique coating architectures and doping and alloying various elements without degrading the mechanical and thermal stability. Interestingly, Yang et al. [13] achieved enhanced tribological properties of AlCrN coatings fabricated on volcano-shaped textured surfaces. These unique structures substantially reduced the real contact of sliding surfaces as well as the wear particles trapped between the textured surfaces, resulting in less frictional force and wear. The sliding mechanisms were rather contradictory at high temperatures, where several fracture deformations and a lower influence of humidity, oxidation process, extreme wear, tribochemical alterations, softening, and third body influences were predominant. Such extreme conditions ultimately require coatings with superior withstanding ability at HT, extreme hardness, and a more precise ability to protect the component against severe wear and oxidations. Worldwide, numerous studies have been conducted on various hard ceramic coatings for high-temperature applications.

Previous research findings are useful for understanding these coatings and advancing the knowledge of utilizing them in various industrial applications. However, due to the huge volume of research, it may be difficult to identify the needed information regarding the selection and application of these coatings. Therefore, the current review focuses on collecting the most essential information required for researchers to understand the recent advancements in hard coatings to be employed in high-temperature applications. We provide a detailed overview of the most recent developments, especially in the last 5 years, regarding the design of hard coatings with the potential to be used in high-temperature applications.

#### *Coating Contact/Failure Mechanisms at Elevated Temperatures*

In recent years, numerous research reports have been made available on different hard coatings for elevated temperature tribological applications [14–18]. The tribological behavior of the coating under HT conditions is evidently different from that under room temperature conditions. Many research reports and a few potential review articles are available regarding the comparative analysis of RT and HT tribological properties of hard

coatings; however, some results only display the RT tribological behavior [19,20]. It is highly necessary to understand the various factors of contact and/or failure mechanisms for coatings that interact with counterbodies at elevated temperatures for any potential application. Based on the literature, it is clearly demonstrated that different contact and/or failure mechanisms occur at the coating/counterbody contact interfaces, as illustrated in the flow diagram in Figure 1. The major wear mechanisms of coatings at elevated temperatures include wear particle adhesion on the interacting surface, abrasive wear, excessive oxidation, phase transformations, chipping, cutting, mechanical property weakening, and coating delamination from substrates [21–23].

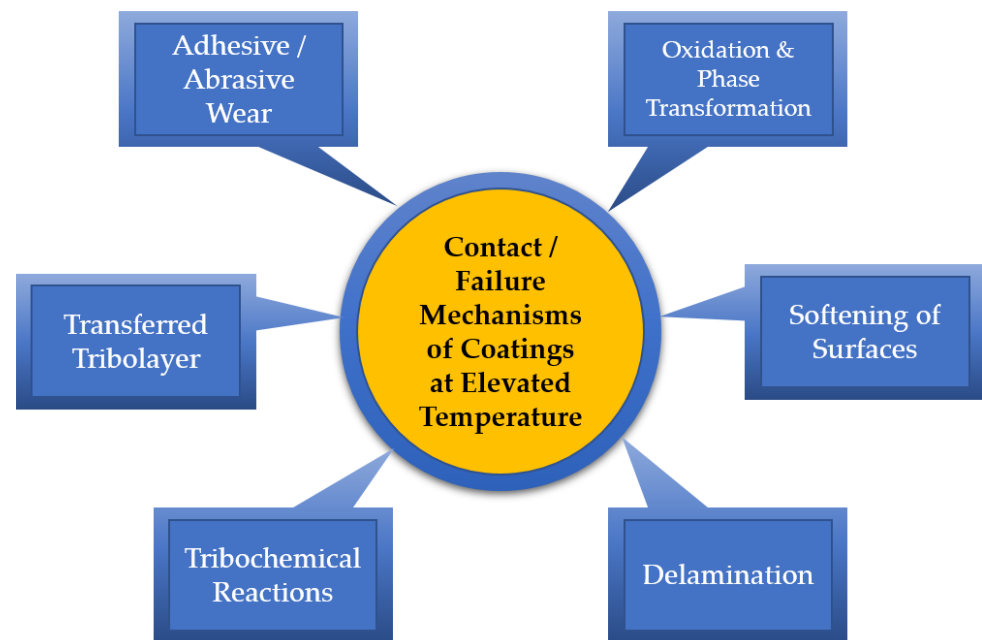


**Figure 1.** Various contact and failure mechanisms are involved during the tribological contact between the coating and counterbodies under high-temperature conditions.

## 2. Hard Refractory Ceramic Coatings for High-Temperature Applications

Nitrides and carbides based on transition metal nitrides have undergone extensive research and development over the last 20 years for use in high-temperature industrial applications. Titanium nitride (TiN) is the primary coating material used for HT applications because of its superior physiochemical and mechanical properties. However, the excessive oxidation of Ti at elevated temperatures (above 550 °C) leads to possible abrasive wear, and deterioration of mechanical hardness limits its applications [24–26].

To overcome this challenge, Al was incorporated into the TiN crystal lattice to create a stable TiAlN phase without changing the crystal structure (typically FCC). The operating temperature of the TiAlN coating was noticeably raised to 1000 °C with a significant increase in mechanical hardness. CrAlN is the other significant high-temperature protective coating material for industrial machining tools owing to its superior oxidation resistance, up to 900 °C. Al-based oxide layers that form on the coatings during HT exposure prevent further oxygen from diffusing inside the material, leading to high temperature stability [27–29]. Depending on the application requirements, the Al concentration was changed by up to 70% to extend the hardness and HT performance of the coatings [30,31]. However, the extremely high friction of these coatings at RT and HT settings severely restricts their use in a variety of industrial applications that demand low-friction properties.

### 3. Fabrication of Hard Ceramic Coatings

#### 3.1. Fabrication Methods

Owing to the ease of operation and superior properties of the coatings, physical vapor deposition (PVD) techniques are the most popular for the deposition of hard ceramic coatings. The most preferable PVD methods for depositing hard coatings include magnetron sputtering, cathodic arc, pulsed laser deposition, and electron beam evaporation. The growth mechanisms of hard coatings are highly dependent on the deposition conditions, plasma kinetics, and physiochemical characteristics of the source elements. Figure 2 shows the many PVD techniques that have been employed over the last five years for fabricating hard coatings, as well as the common deposition parameters that affect the characteristics and functionality of the coatings. Among many PVD methods, magnetron sputtering methods are the most widely used techniques for fabricating hard coatings, owing to the ease of controlling the stoichiometry, microstructure, mechanical properties, and highly dense, defect-free, uniform structure of the coatings by controlling various processing parameters, such as ion energy, ion flux, sputtering power, substrate bias, gas flow rate, partial pressure, and substrate temperature [32].

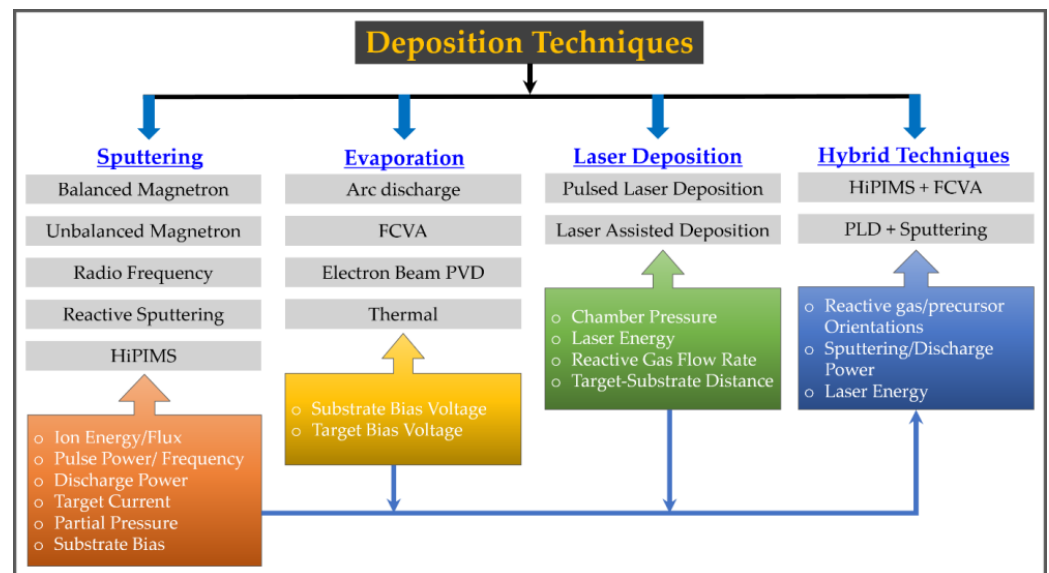


**Figure 2.** PVD methods to deposit hard ceramic coatings and the major process parameters influencing the coating properties.

Many types of advanced sputtering techniques, including balanced magnetron sputtering, radio frequency, reactive sputtering, and high-power impulse magnetron sputtering (HiPIMS), are frequently used for fabricating hard coatings. Owing to its ability to manufacture highly dense, stable, and hard coatings, HiPIMS is presently used as a flexible technology to deposit hard ceramic coatings for tribological applications [11,33–37]. Other potential techniques for fabricating materials for extreme environmental applications, such as filtered cathodic vacuum arc (FCVA) [38,39], pulsed laser deposition (PLD) [40,41], and their hybrid approaches with magnetron sputtering [42–44], have been used extensively in recent years. Figure 2 also includes the crucial parameters for tuning the microstructure and mechanical properties of the coatings produced by various PVD techniques.

The schematic representations of current coating techniques are shown in Figure 3, including filtered cathodic vacuum arc (FCVA), hybrid vacuum arc with RFMS, hybrid radio frequency magnetron sputtering (RFMS), HiPIMS, and ultrashort PLD. For the fabrication of ZrSiN coatings, Chang et al. [45] employed the co-sputtering approach of RFMS/HiPIMS (as depicted in Figure 3a). Owing to the combined ability of forming a denser coating morphology by HiPIMS and grain refinement by the addition of Si through RFMS, the residual stress of the coatings was reduced, and the resulting increase in hardness and

elastic modulus were the most promising properties for use in extreme environmental applications. Pulsed laser deposition is another popular method for creating hard coatings (Figure 3b) [46,47]. Atoms from the source material are evaporated in this process using a high-energy, ultra-short, pulsed laser beam. As the atoms migrate toward the substrate, they produce a homogeneous layer. Furthermore, stoichiometry control from the source material to the coatings is superior using the PLD method compared to the other techniques, enabling the development of unique coatings with the desired compositions [48].

Figure 3c shows a schematic of the FCVA deposition system, where the substrates (anode) are mounted inside the vacuum chamber, while the target (cathode) is mounted at another end of the filter arch. To avoid larger particle and droplet formation in the coating, typically C-bend or S-bend arches are used in the FCVA system. Cao et al. [49] developed a multilayer coating of Ti-DLC on an Al alloy substrate using the FCVA method that exhibited ultralow friction (0.12), improved wear resistance ( $2.69 \times 10^{-7} \text{ mm}^3/\text{Nm}$ ) at  $300 \text{ }^\circ\text{C}$ , and decreased thermal conductivity, which could be beneficial for engine piston assemblies. However, hard coatings produced by cathodic arc methods frequently contain surface droplets that cause friction and wear during the initial period of sliding. Panjan et al. [50] revealed that post-polishing procedures for cathodic arc-deposited TiN coatings could improve the wear resistance and shorten the running-in duration. Another interesting fabrication method is the combined vacuum arc and magnetron sputtering hybrid process described by Hirata et al. [51], as shown in Figure 3d, for creating amorphous boron carbon nitride (a-BCN) films for tribological applications. Here, the BN target is mounted on the RFMS, while the graphite target is positioned on the cathodic arc gun to deposit the films. The use of a vacuum arc in the hybrid technique enhances the ionization rate and the kinetic energy of sputtered atoms/particles which bombard the substrate. Moreover, the diagonal placement of the arc gun in relation to the substrate allows for better control of droplet deposition in the coatings, a common problem associated with conventional vacuum arc processes.

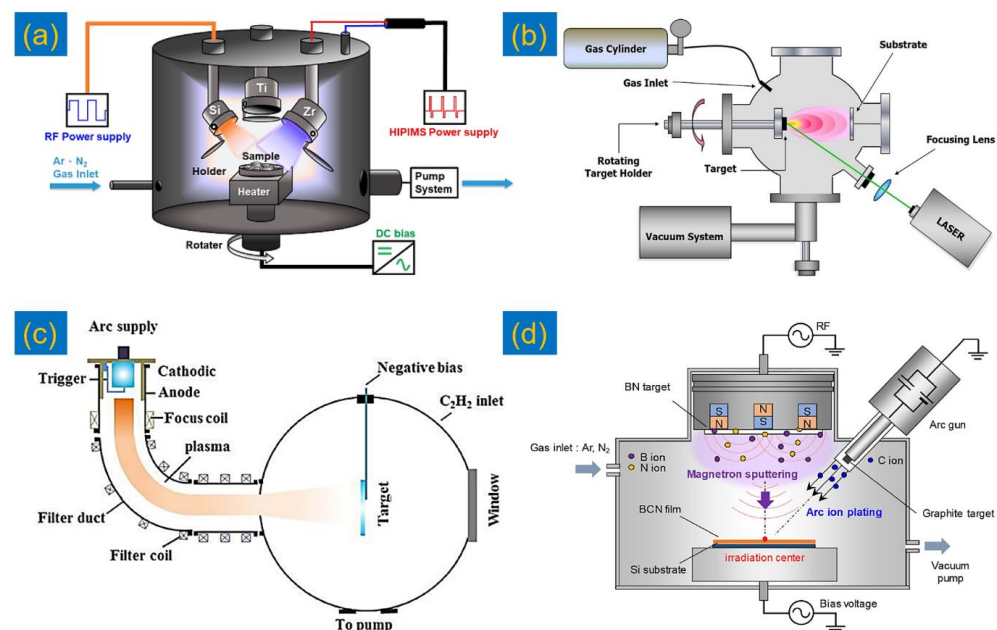


**Figure 3.** Schematic of the advanced PVD deposition methods used for the fabrication of cutting-edge hard coatings for tribological applications. (a) Co-sputtering method of RFMS and HiPIMS [45], (b) ultra-short PLD [46], (c) FCVA [49], and (d) arc-sputtering hybrid method [51]. (Reproduced with permission.)

### 3.2. Binary, Ternary, and Multicomponent Ceramic Coatings

Coating microstructures can be engineered to improve their properties by tailoring the deposition parameters of PVD techniques. Binary and ternary coatings have been most widely studied over the past few decades for a variety of industrial applications, including small-scale devices and large-scale mechanical components. In the last ten years, significant breakthroughs in coating concepts have been developed and investigated in the search for improved characteristics and long-lasting coatings for extreme environmental applications. Multicomponent, multilayer, nanocomposite, and functionally graded coatings have received much attention globally during the past five years [52–56]. Recent research trends indicate a notable interest in the development of multicomponent coatings by co-depositing or evaporating compound target materials in an atmosphere of reactive nitrogen ( $N_2$ ). The introduction of elements into the crystalline lattice was developed to refine the grain growth and thereby enhance the mechanical strength and wear resistance in extreme sliding conditions [57,58]. For instance, Rodríguez et al. [59] observed a hardness enhancement from 32 GPa to 36 GPa for a small fraction (0.2 at%) of Hf doped into  $Al_xTi_{1-x}N$  coatings to form  $c-Al_{0.64}Ti_{0.36}Hf_{0.02}N$  coatings using the cathodic arc method. They suggested that the oxidation temperature of the coating was increased to 900 °C owing to the addition of Hf, which forms Hf-based oxynitrides and Al/Ti-based oxide layers during HT exposure. On the other hand, a study by Grigoriev et al. [60] showed that Ti-TiN-(Ti, Al, Nb, and Zr)N multicomponent coatings significantly enhanced the wear resistance and reduced the friction and performance of cutting tools with increasing the temperature from 700 to 900 °C.

On the other hand, the multilayered coatings showed remarkably improved properties, such as hardness, fracture toughness, and elastic modulus, compared to the single-layer coatings. It was revealed that a number of multilayer structures with varied compositions between sublayers improved the mechanical properties. The interface/superlattice structures between two alternate layers in this case impede the mobility of plastic deformation, acting as dislocation gliding barriers [61,62]. Xiao et al. [63], for example, achieved a maximum hardness of 38.3 GPa and an elastic modulus of 463.7 GPa, as well as the highest thermal stability (up to 1000 °C) and wear resistance at 800 °C, for the AlCrN/TiAlSiN multilayer compared to single-layer coatings. The multilayer structure, as well as the unique nanocomposite structure of the  $Si_3N_4$  matrix around the TiAlN crystals from the TiAlSiN layers, were responsible for these properties. Similar enhanced mechanical and tribological properties of different multilayer architectures, such as CrAlN/TiSiN [64], AlCrSiN/VN [65], TiAlSiN/VSiN [66], and AlCrN/TiAlSiN [63], have been reported. The consolidated mechanical and HT tribological performances of multicomponent and multilayer coatings are described in Table 1.

**Table 1.** Recent developments in hard coatings for high-temperature tribological applications from publications in the last five years.

Coating	Deposition Method/Post Treatments	Thickness ( $\mu\text{m}$ )	Mechanical Properties (GPa)	Tribological Properties at HT	Major Outcomes	Ref.
<b>Multicomponent and nanocomposite hard ceramic coatings fabricated using PVD techniques for HT tribological applications</b>						
AlTiVCuN	HiPIMS	1.0–1.6	H: 34–41 GPa	$\mu$ : 0.5 $k$ : $3.2 \times 10^{-15} \text{ m}^3/\text{Nm}$ (600 °C)	Cu rich coating involved more outwards diffusion of Cu to form the lubricious CuO at HT As a result of very compact morphology of nanocomposite coatings, detachment of larger hard W–C particles is prevented, resulting in low-friction and higher wear resistance	[67]
W-DLC	Hybrid DCMS + HiPIMS	1.7	E: 200 GPa	$\mu$ : 0.1 $k$ : $2 \times 10^{-7} \text{ mm}^3/\text{Nm}$ (150 °C)		[68]
Al <sub>2</sub> O <sub>3</sub> /ta-C	Lateral Arc with Central Sputtering and ALD for Al <sub>2</sub> O <sub>3</sub> layer	(ta-C) and 200 nm (Al <sub>2</sub> O <sub>3</sub> top layer)	–	$\mu$ : 0.1 (500 °C) Wear Volume: $1.4 \times 10^{-3} \text{ mm}^3$ (500 °C)	The suppression of oxidation by a thin Al <sub>2</sub> O <sub>3</sub> multifunctional layer improves the thermal stability and durability of the ta-C coating.	[69]
(Cr, V)N	Cathodic Arc ion-plated	4.5	H: 24 GPa	$\mu$ : 0.28–0.37 Wear Volume: $1.4\text{--}12.9 \times 10^{-5} \text{ mm}^3/\text{Nm}$ (700–900 °C)	Because of the formation of V–O phases, Cr <sub>0.58</sub> V <sub>0.14</sub> N <sub>0.28</sub> coatings demonstrated superior tribological properties at 700–800 °C	[70]
AlCrON, and $\alpha$ -(Al,Cr) <sub>2</sub> O <sub>3</sub>	Cathodic Arc	4.0	H: 34.6 GPa E: 467 GPa (AlCrON) H: 26 GPa E: 446 GPa ( $\alpha$ -(Al,Cr) <sub>2</sub> O <sub>3</sub> )	$\mu$ : 0.5 $k$ : $150 \times 10^{-17} \text{ m}^3/\text{Nm}$ (AlCrON at 800 °C) $\mu$ : 0.25 $k$ : $10 \times 10^{-17} \text{ m}^3/\text{Nm}$ ( $\alpha$ -(Al,Cr) <sub>2</sub> O <sub>3</sub> at 800 °C)	Superior tribological properties of the $\alpha$ -(Al,Cr) <sub>2</sub> O <sub>3</sub> coating due to the nitrogen-free, stable alpha-alumina structure that inhibited HT oxidation and subsequent wear	[22]
Cr-V-Al-C	Hybrid Arc and Magnetron Sputtering	7.5	H: ~22.5 GPa E: ~280 GPa	$\mu$ : 0.5 $k$ : No measurable wear (900 °C)	The formation of a combined Cr <sub>2</sub> O <sub>3</sub> and Al <sub>2</sub> O <sub>3</sub> tribolayer can be favored by optimizing the solid solution content of V in Cr <sub>2</sub> AlC coating, leading to high hardness and HT tribological performance At 400 °C, formation of mixed lubricious oxides of MoO <sub>3</sub> /CuMoO <sub>4</sub> and V <sub>2</sub> O <sub>5</sub> decreases the wear resistance compared to tests conducted at RT due to the loss of N and severe oxidation at HT	[71]
MoCuVN	HiPIMS	2.1–2.4	H: 19.0–15.5 GPa E: 393–316 GPa (with increasing N <sub>2</sub> flow rate)	$\mu$ : 0.43–0.51 $k$ : $3.1\text{--}13.5 \times 10^{-8} \text{ mm}^3/\text{Nm}$ (400 °C)		[72]
<b>Multilayer hard ceramic coatings fabricated using PVD techniques for HT tribological applications</b>						
CrAlN/TiSiN	Arc Ion Plating	6.8	2850 HV	$\mu$ : 0.6 $k$ : $3.95 \times 10^{-6} \text{ mm}^3/\text{Nm}$ (300 °C)	Coatings are highly stable at high temperatures, while the adhesive wear of the ball on the coating surface forms the Fe <sub>2</sub> O <sub>3</sub> tribolayer Improved tribological properties due to improved mechanical properties and the formation of a self-lubricating V <sub>2</sub> O <sub>5</sub> Magnéli phase at 700 °C	[73]
TiAlSiN/VSiN	RF magnetron co-sputtering	1.0–1.2 (10–40 nm bilayer periods)	H: 29 GPa E: 260 GPa	$\mu$ : 0.28 $k$ : $7.01 \times 10^{-6} \text{ mm}^3/\text{Nm}$ (700 °C)		[74]
CrMoN/SiN <sub>x</sub>	RF magnetron co-sputtering	1.2 (1 nm SiN <sub>x</sub> and 10–200 nm CrMoN)	H: 27 GPa E: 200 GPa (for 100 nm CrMoN/1 nm SiN <sub>x</sub> )	$\mu$ : 0.22 $k$ : $1.68 \times 10^{-5} \text{ mm}^3/\text{Nm}$ (600 °C)	The optimal thickness of bilayer periods and laminated architecture for stress dispersal and deflection results in improved performance	[66]
AlCrSiN/VN	Arc Ion Plating and Pulsed DC Sputtering	3.0 (4.6 nm modulation period)	H: 30.7 GPa (Multilayer) H: 28 GPa (AlCrSiN) H: 20.5 GPa (VN)	$\mu$ : 0.26 (800 °C) $k$ : $2.6 \times 10^{-15} \text{ m}^3/\text{Nm}$ (600 °C) & $39.4 \times 10^{-15} \text{ m}^3/\text{Nm}$ (800 °C)	Outwards diffusion of V and Al to form V <sub>2</sub> O <sub>5</sub> and AlVO <sub>4</sub> phases results in low friction and increased wear resistance at HT	[65]
AlCrN/TiAlSiN	Cathodic Arc	2.2	H: 38 GPa E: 463 GPa	$\mu$ : 0.45 (800 °C) $k$ : $2.5 \times 10^{-6} \text{ mm}^3/\text{Nm}$ (800 °C)	Enhanced wear resistance is provided by the formation of a dense Al <sub>2</sub> O <sub>3</sub> oxide lubricant layer on the wear tracks	[63]
TiN-AlTiN/nACo-CrN/AlCrN-AlCrOAlTiCrN	Cathodic Arc	3.6	H: 36–41 GPa	$\mu$ : 0.45 (800 °C)	The formation of stable protective oxides ((Al,Cr) <sub>2</sub> O <sub>3</sub> ) increases the wear resistance at 800 °C compared to 600 °C	[75]

### 3.3. Significance of the Structural and Mechanical Properties of Ceramic Coatings

The tribological properties of hard coatings are primarily governed by several internal factors of coatings, including compositional, structural, microstructural, and mechanical properties, as well as other external factors, such as the sliding atmosphere, load, sliding speed, and humidity. The microstructure of the coating can be tailored to enhance the mechanical and HT properties depending on the concentration of added components in

the primary phases of the coating. For the  $\text{Al}_{60}\text{Cr}_{30}\text{Si}_{10}$  compound target, Fan et al. [76] observed a gradual change in Al and Si composition with a periodic change in sputtering power from 0.6 to 1.2, then to 2.0, and finally to 2.8 kW. They also observed the variation in crystallinity and microstructure of quaternary CrAlSiN coatings with the change in sputtering power from 0.6–1.2, then to 2.0, and finally to 2.8 kW. The coating samples deposited at 0.6–2.8 kW displayed poor wear resistance due to weaker crack resistance and higher surface roughness, whereas the highly dense and smooth surface coatings deposited at 0.6–2.0 kW exhibited improved wear resistance. To compare the microstructure and morphologies of CrN coatings, Ferreira et al. [77] developed two different coatings under varying process conditions of  $\text{N}_2$  gas flow, partial pressure, and bias voltage. With a low  $\text{N}_2$  gas flow and partial pressure with a higher bias voltage, a highly dense, void free, enhanced hardness microstructure coating with low friction (0.15) and wear loss was achieved. A second coating was deposited at higher  $\text{N}_2$  and lower bias voltage, and the friction and wear loss were higher because of the presence of more voids inside the coating. Substrate rotational speed during the sputtering deposition of hard coatings also has a significant impact on the microstructure and mechanical properties of hard coatings. With increasing rotation speed, the dense microstructures are transferred to the coarse microstructure. The film growth direction and the mobility of adatoms during sputtering are greater at lower rotational speeds due to the almost perpendicular position of sputtered ions to the film growth surface, resulting in a dense microstructure. At higher speeds, the angle of growth of the coating structure predominantly varies, reducing the energy of sputtering ions [78]. Wang et al. [79] investigated the effect of reactive  $\text{N}_2$  partial pressure on TiBN/TiAlSiN nano-multilayered coatings fabricated by the cathodic arc technique. The coating deposited at 2.0 Pa partial pressure had a defect-free, smoother surface and a dense microstructure, resulting in improved hardness (34 GPa), H/E, and  $\text{H}^3/\text{E}^2$ ; low friction (0.28); and wear resistance ( $4.3 \times 10^{-7} \text{ mm}^3/\text{Nm}$ ). A higher partial pressure (3.0 Pa) caused target poisoning and a reduction in coating thickness.

Similarly, changing the bias voltage causes significant changes in the tribological properties of cathodic arc-deposited ternary and quaternary nitride coatings [80,81]. Cao et al. [82] observed a change in the preferred orientation from (200) to (111) for TiAlN coatings deposited using FCVA when the bias voltage was increased from 50 to 75 V. This is due to an increase in atomic mobility and lattice distortion, which results in a higher hardness ( $\sim 30.3$  GPa) and wear resistance ( $\sim 4.4 \times 10^{-5} \text{ mm}^3/\text{Nm}$ ). Akhter et al. [83] achieved a remarkable 85% increase in wear resistance for arc-produced TiNiN coatings at a 100 V bias voltage rather compared to the coating deposited at 0 V. The enhanced mechanical and tribological properties in this case were due to the very fine equiaxed structure and higher compressive residual stress. A similar improvement in tribological performance was observed for CrN/NbN multilayers deposited via HiPIMS with substrate biases ranging from  $-40$  to  $-150$  V [84]. The coating deposited at  $-65$  V demonstrated reduced friction and enhanced wear resistance owing to the increased density of columnar grains. However, a higher substrate bias caused grain coarsening and increased defect concentration, which increased friction and wear. It is clear that the coating microstructure, thickness, composition, roughness, hardness, and toughness are clearly influenced by the applied substrate bias voltage. Therefore, the optimum bias voltage during PVD coating deposition plays a critical role in reducing internal stress and improving load-bearing ability. Interlayer thickness, on the other hand, has a significant impact on the residual stress and wear properties of hard coatings, according to Lin et al. [85]. They observed that increasing the Ti interlayer thickness of TiZrN coatings from 50 to 250 nm decreased the residual stress from  $-5.67$  to  $-3.75$  GPa, and the wear resistance increased by 16%.

#### 4. Recent Progress in Advanced Coatings for Application in Harsh Environments

Many researchers around the world have designed and developed several hard coatings in the last five years to improve load-bearing ability under extreme environmental conditions. The majority of researchers are concerned with tailoring the microstructure by

adding appropriate elements to achieve adaptive coatings with multifunctional properties. Many researchers are interested in multicomponent coatings and novel multilayer structures, as previously discussed. Table 1 shows the recently developed advanced coatings deposited using PVD methods, as well as their mechanical and tribological properties, particularly under harsh operating conditions.

#### 4.1. Recent Advancements in Coating Design Aspects

The improved design of hard coatings shows beneficial effects on the mechanical and tribological properties of coatings through controlling the microstructure, varying the composition, altering the nanocomposite design, and combining hard/soft multilayer coatings. Figure 4 depicts the various coating architectures that have been created using PVD methods for use in HT environments. For the selection of hard coatings to extend the performance and life of the base components, there are several primary concerns. Considering the extreme mechanical hardness of the coating, the influence of internal stress would limit the coating's adhesion properties to the substrate, resulting in delamination during highly stressed sliding operations. Therefore, special coating architectures are highly inevitable, with specific properties at different zones for HT tribological applications. Figure 4 depicts the coating concept with desirable properties at different zones, such as higher adhesion strength between the coating and substrate (zone 1), a mechanical layer with high fracture toughness and wear resistance in the middle (zones 2 and 3), and active surface layers (zone 4) that should provide lubricity and superior oxidation resistance properties.

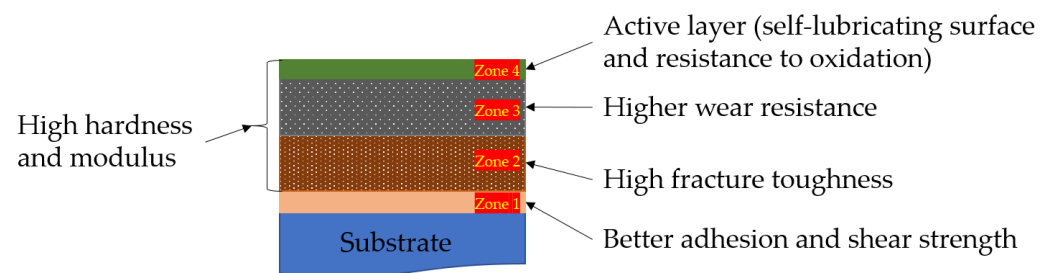


**Figure 4.** Schematic representation of the advanced coatings with important properties at different zones for high-temperature tribological coatings.

Many researchers have reported different coating architectures using PVD techniques in the last five years, taking into account the above coating requirements for extreme environmental applications. Figure 5 depicts the most recent coating architectures studied for HT tribological applications from the literature. Haung et al. [86] designed gradient composite TiAlSiN coatings and achieved improved tribological performance as well as superhardness (42 GPa) and superior adhesion strength (85 N). Figure 5a depicts the three-layer microstructure of this coating, where TiN and AlTiN provide mechanical stability, while the formation of SiO<sub>2</sub> surface oxides from the top TiAlSiN layer improves lubrication and protection efficiency. In another study, multicomponent gradient (Ti, Al, Si, Cr, Mo, S, O, and N) coatings (Figure 5b), fabricated using UBMS, demonstrated improved tribological performance due to the presence of many nanocrystalline phases, which effectively impeded the deformation during sliding [87]. Bondarev et al. [88] developed TiSiN/TiN(Ag) multilayer coatings using DCMS with a total thickness of 2.3 μm and a bilayer thickness of 40 nm for tribological applications. Chang et al. [89] fabricated novel multilayer AlTiN/CrN/ZrN coatings using a cathodic arc, as shown by the cross-sectional TEM micrograph, for tribological applications. They observed that fabricating an AlTiN/CrN/ZrN multilayer greatly reduced residual stress, resulting in superior wear resistance ( $4.21 \times 10^{-7} \text{ mm}^3/\text{Nm}$ ).

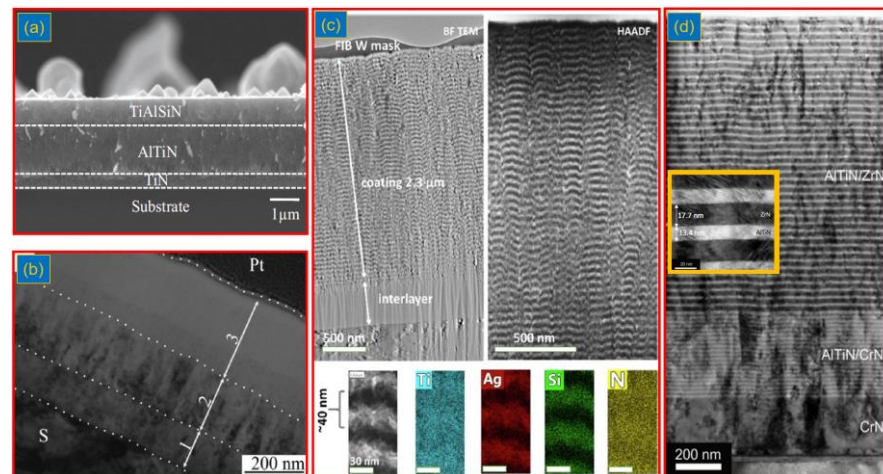


**Figure 5.** Cross-sectional microstructure of various coating architectures in the recent literature. (a) FESEM micrograph of a three-layer TiN/AlTiN/TiAlSiN coating [86], (b) bright field HRTEM image of a gradient layered structure (Ti, Al, Si, Cr, Mo, S, O, and N) coating [87], (c) bright field TEM, HAADF STEM, and EDS elemental distribution of TiSiN/TiN(Ag) multilayer coatings [88], and (d) TEM micrograph of novel nanoscale multilayered CrN/[AlTiN/CrN]<sub>n</sub>/[AlTiN/ZrN]<sub>n</sub> coatings [89]. (Reproduced with permission.)

As a result, in recent studies, the main consideration to improve the tribological performance of hard ceramic coatings is mainly controlled by tailoring the coating microstructure by introducing additional elements and/or fabricating new coating architectures. The selected additive materials should possess solubility in the primary coating to some extent, be able to form strong protective oxides on the coating surface during HT sliding conditions, control the inwards diffusion of oxides, and promote self-lubricating effects. In the case of multilayer coatings, the interface strengthening mechanism with periodic changes between sublayers exhibits enhanced resistance to plastic deformation and wear even at high temperatures. Several metals, nonmetals, and soft metals have been considered for this purpose in recent research, and the advancements in these nanocomposite and multicomponent coatings for HT applications are described in the following sections.

#### 4.2. Role of Dopants (Mo, Cr, W, Si, and C) in Hard Ceramic Coatings

As a result of their superior mechanical stability over a wide operating temperature range, nanocomposite coatings have recently received much attention for high-temperature tribological applications. However, there is still a problem associated with the lack of high-temperature lubricity of nanocomposite coatings compared to at room temperature, resulting in poor wear lifetime. To address this issue, transition metal-based dopants such as Ti, Mo, V, and W, as well as nonmetallic elements such as Si, C, and B, have been used to improve the tribological performance at elevated temperatures. The formation of the Magnéli phase of transition metal oxides with layered crystal structures during exposure of these metals to high-temperatures provides an improved load-bearing ability at high temperatures. These layered structures slip more easily during sliding motion, providing enhanced lubrication due to their attenuated Van der Waals forces between each layer's crystal. For example, Tao et al. [90] discovered that adding Mo to magnetron-sputtered CrAlSiN coatings reduced the friction with increasing Mo concentration. They observed that the stable MoO<sub>3</sub> species, observed in the tribolayer in ESCA analysis, which provides the self-lubrication properties of nanocomposite CrAlMoSiN coatings at 600 °C, is more stable than the CrAlSiN coatings.

Another study found that adding Mo and C to the TiN crystalline lattice significantly improved the mechanical and tribological properties. In this case, Mo addition promoted hardness and toughness by increasing the crystallite charge density as well as forming Magnéli phases, and C addition promoted the formation of amorphous carbon (a-C) phases

at grain boundaries, resulting in friction reduction and wear resistance [91]. Similarly, Cr-rich additions to TiAlN-coated tools provided a greater cutting performance above 600 °C due to the formation of a protective Cr-O tribolayer, which is the strongest tribolayer, compared to Al-O and Ti-O gained from TiAlN coatings at higher cutting speeds [92]. Similar behavior of WO<sub>3</sub> triboinduced oxides at high temperatures for the addition of W in magnetron-sputtered HfN coatings with diverse additive compositions revealed minimal friction and wear resistance at high temperatures [93]. However, excessive amounts of these transition metals are prone to oxidative damage at high temperatures.

As previously stated, oxidation of coatings plays a critical role in the formation of tribolayers on interacting surfaces in the HT environment. Metal oxides, depending on their nature, may be prone to abrasive and third body wear, as well as some protective oxides that are stable under extreme temperature conditions. For example, TiO<sub>2</sub> formation from TiAlN coatings under HT (typically above 600 °C) provides lubricity, but these oxides have poor wear resistance. In contrast, the formation of Al- and Cr-based oxides in CrAlN coatings provides superior wear resistance at extremely high temperatures (900 °C) but with relatively high friction [94,95]. In this regard, adding a small fraction of Si to TiAlN coatings may prevent Ti from diffusing out of the coating, thereby improving oxidation and wear resistance. The formation of a stable Si<sub>3</sub>N<sub>4</sub> structure in the TiAlSiN coating, depending on the Si concentration, significantly improves the mechanical and tribological properties. However, excessive Si addition will cause the coatings to become brittle, resulting in increased friction and wear.

Drnovšek et al. [96] investigated the correlation between HT mechanical and tribological properties for the addition of Si in CrAlN coatings using the magnetron sputtering method. The mechanical and tribological properties of the CrAlSiN coatings were superior to those of CrAlN coatings from RT to HT (up to 700 °C). However, the mechanical properties decreased with increasing temperature during indentation (H: 37 GPa to 36 GPa for CrAlSiN and 31 GPa to 24 GPa for CrAlN). Figure 6a depicts the comparison of the observed friction and wear rates for both coatings tested from RT to 700 °C. The friction increases in both coatings at intermediate temperatures up to 500 °C due to the formation of wear debris and third body wear. Comparatively, wear predominates in the CrAlN coatings, as shown in Figure 6b, where abrasive wear of oxides and three body wear predominate. However, wear resistance was superior for the CrAlSiN coatings, as shown in Figure 6c, due to the enhanced resistance to oxidation and a critical H/E\* ratio of 0.08–0.085 at HT, resulting in improved wear resistance. As a result, they suggested that optimizing the H/E\* ratio of the coatings could be the critical governing parameter for the wear resistance characteristics.

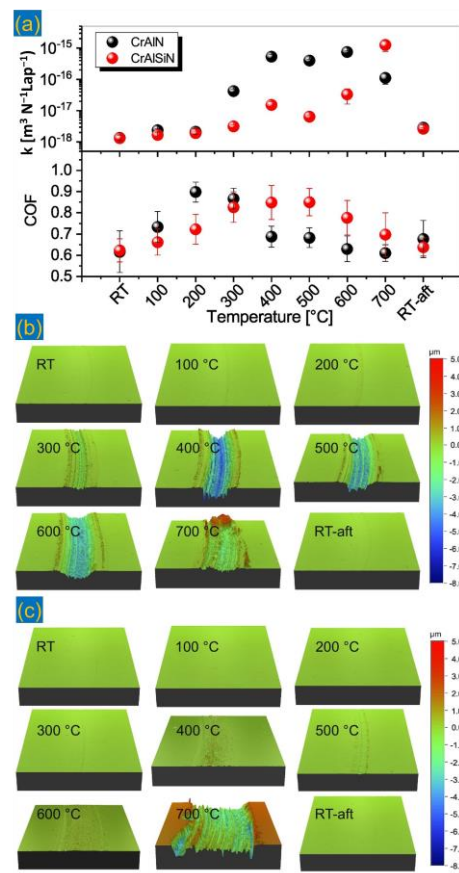


**Figure 6.** (a) Friction curves of CrAlN and CrAlSiN coatings tested under inert atmosphere at elevated temperature (RT to 700 °C). 3D optical profiler images of the wear tracks of (b) CrAlN and (c) CrAlSiN coatings after testing from RT to 700 °C [96]. (Reproduced with permission.)

Cai et al. [97] investigated the effect of B addition to AlCrN coatings using the arc ion plating method for high-temperature tribological applications. For this, they fabricated a coating with Cr and CrN layers on the substrate, followed by an AlCrN layer, then by the incorporation of B in the top layer with different B contents of 1.5 at%, 2.9 at%, and 4.8 at% to obtain the AlCrBN top layer. They found that a solid solution of B in the AlCrN columnar structure at 1.5 at% and a small fraction of a-BN<sub>x</sub>, as seen in the TEM microstructure and schematic (Figure 7a,d), resulted in superior hardness (38.3 GPa) and modulus (622 GPa). When the B content exceeded 2.9 at%, composite (Al, Cr, and B)N nanograins and a-BN<sub>x</sub> composite structures were formed and crystallinity decreased, as shown in Figure 7b,c,e,f. This was followed by a decrease in the mechanical properties to 26 GPa (H) and 389 GPa (E\*). The HT tribological results showed that the B content of 4.8 at% had superior wear resistance at 800 °C due to the formation of continuous tribofilms on the wear tracks. Figure 7g depicts the different tribological mechanisms of AlCrBN (4.8 at%) coatings with respect to temperature change based on the wear track micrograph and tribochemical analysis. Continuous Cr<sub>2</sub>O<sub>3</sub> tribofilms were observed at 400 °C, while at 600 °C, continuous Al<sub>2</sub>O<sub>3</sub> and Cr<sub>2</sub>O<sub>3</sub> with a small fraction of discontinuous B<sub>2</sub>O<sub>3</sub>/B(OH)<sub>3</sub> tribofilms were obtained, and at 800 °C, a stable and continuous B<sub>2</sub>O<sub>3</sub>/B(OH)<sub>3</sub> tribofilm was formed as a protective layer of the coating from wear. Korneev et al. [98] also observed improved mechanical, HT tribological, and oxidation resistance with C and N doping, when they fabricated TaZrSiBCN hard coatings through a sputtering technique.

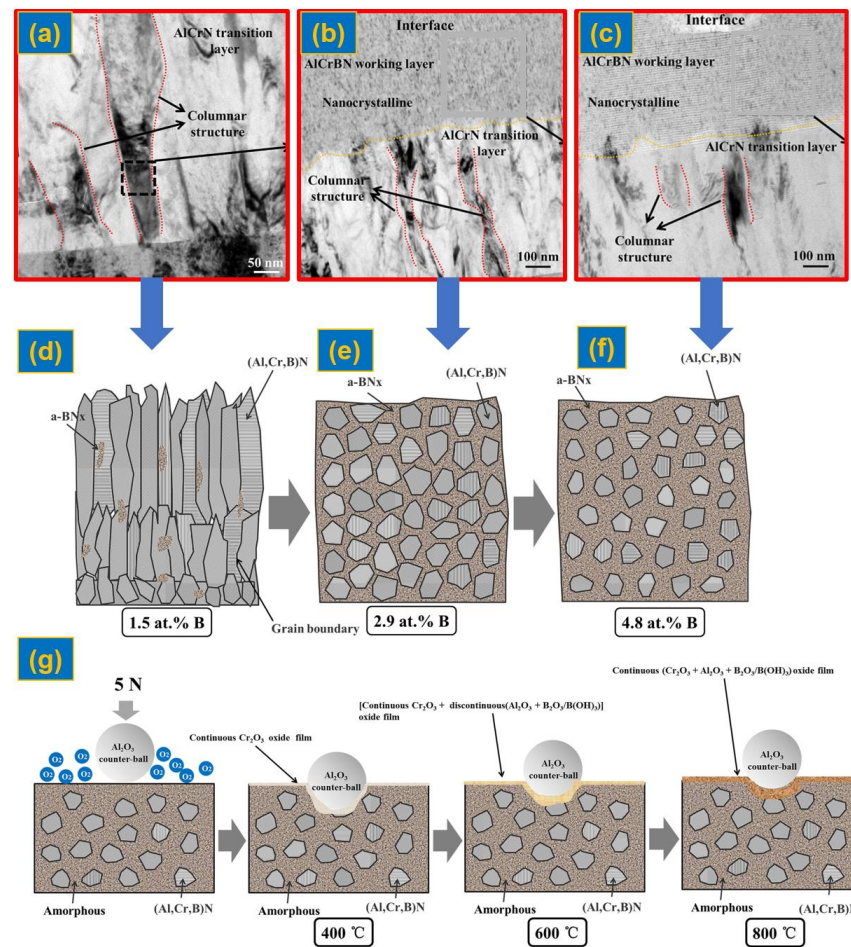


**Figure 7.** TEM microstructure and corresponding schematic representation of the AlCrBN coatings with B contents of (a,d) 1.5 at%, (b,e) 2.9 at%, and (c,f) 4.8 at%. (g) Schematic of the wear mechanism of the AlCrBN coating with 4.8 at% B at different temperatures (RT–800 °C) [97]. (Reproduced with permission).

#### 4.3. Soft/noble Metal (Ag and Cu)-Doped Hard Coatings for High-Temperature Applications

Another promising coating design concept for elevated-temperature tribological applications is the incorporation of soft/noble metals into hard ceramic coatings. In recent years, metals such as Ag, Au, and Cu have been incorporated as a second phase as well as a lubricant phase into hard nitride coatings to form a nanocomposite structure (nc-MeN/metal) to improve high-temperature tribological properties. These materials not only have improved fracture toughness and hardness due to grain refinement but also have an excellent lubrication effect due to out-diffusion of soft metals at high temperatures [99]. The morphologies and microstructures of soft metals (Ag and Ag-Cu) doped into hard coatings for tribological applications are depicted in Figure 8a–c. The microstructure of the coatings substantially varies depending on the dopant concentration, beginning with the formation of a solid solution in the primary crystal lattice and progressing to nanosized grains at lower concentrations. The microstructure of the coating is altered or amorphized with higher concentrations of soft metals (Ag and Cu), and larger particles are then out diffused onto the coating's surface. Figure 8d illustrates the change in the microstructure with varying Ag content from 0 to 25.3 at%; the columnar microstructure disappears, and the amorphous structure predominates, which accelerates wear at high temperatures [100].

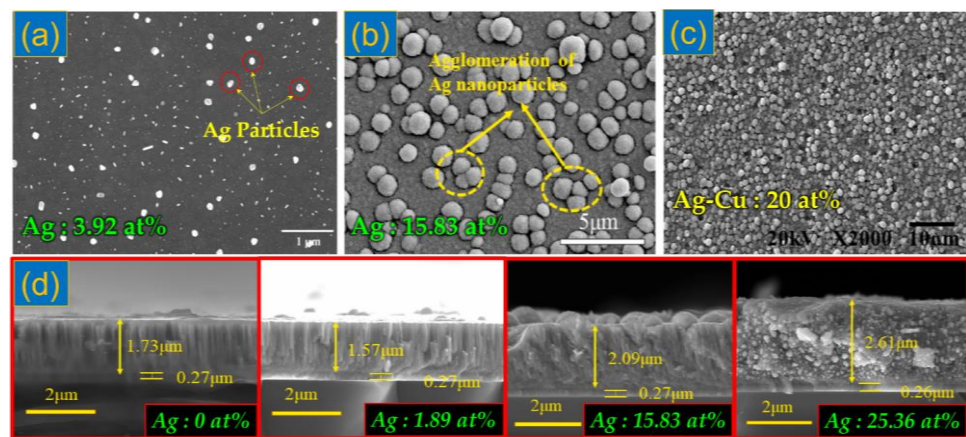


**Figure 8.** Microstructure of soft metal doping/addition to hard ceramic coatings. SEM morphologies of (a) CrMoSiCN coatings with Ag doping (3.92 at%) [101], (b) nanocomposite NbN-Ag coatings (Ag content of 15.83 at%) [102], and (c) Ag-Cu incorporated TiAlN coatings (Ag-Cu contents of 20 at%) [102]. (d) Growth morphologies of NbN-Ag (Ag content 0, 1.89, 15.83, and 25.36 at%) [100]. (Reproduced with permission.)

Recently, Rajput et al. [103] conducted a comparative tribological performance analysis of CrAlN coatings with Ag additions ranging from 2.4 at% to 15.6 at%. They observed that adding Ag up to 8.6 at% increased the mechanical hardness from 18 GPa to 23 GPa due to grain refinement, but it tended to decrease (to 14.4 GPa) with further Ag addition due to the enrichment of softer phases. The friction and wear resistance characteristics did not change significantly at room temperature, but there was a more than two-fold reduction in low-friction values for coatings with higher Ag concentrations (9–16 at%) at elevated temperature (600 °C), as shown in Figure 9a,b. Such enhancement in lubricity is anticipated from the Ag- and AgCrO<sub>2</sub>-rich tribolayers on the wear tracks of these samples, as represented in the FESEM and EDX analysis (Figure 9c–g). The self-lubricating properties are caused by the outwards diffusion of Ag at high temperatures. However, the wear resistance and mechanical properties of higher Ag content (12 and 16 at%) samples were drastically reduced due to the excessive presence of soft phases, as seen in the wear micrographs and EDS results. They found that the optimal addition of Ag (9 at%) shows low friction and improved wear resistance at HT (600 °C) due to the formation of Ag and AgCrO<sub>2</sub> (as seen in Figure 7e).

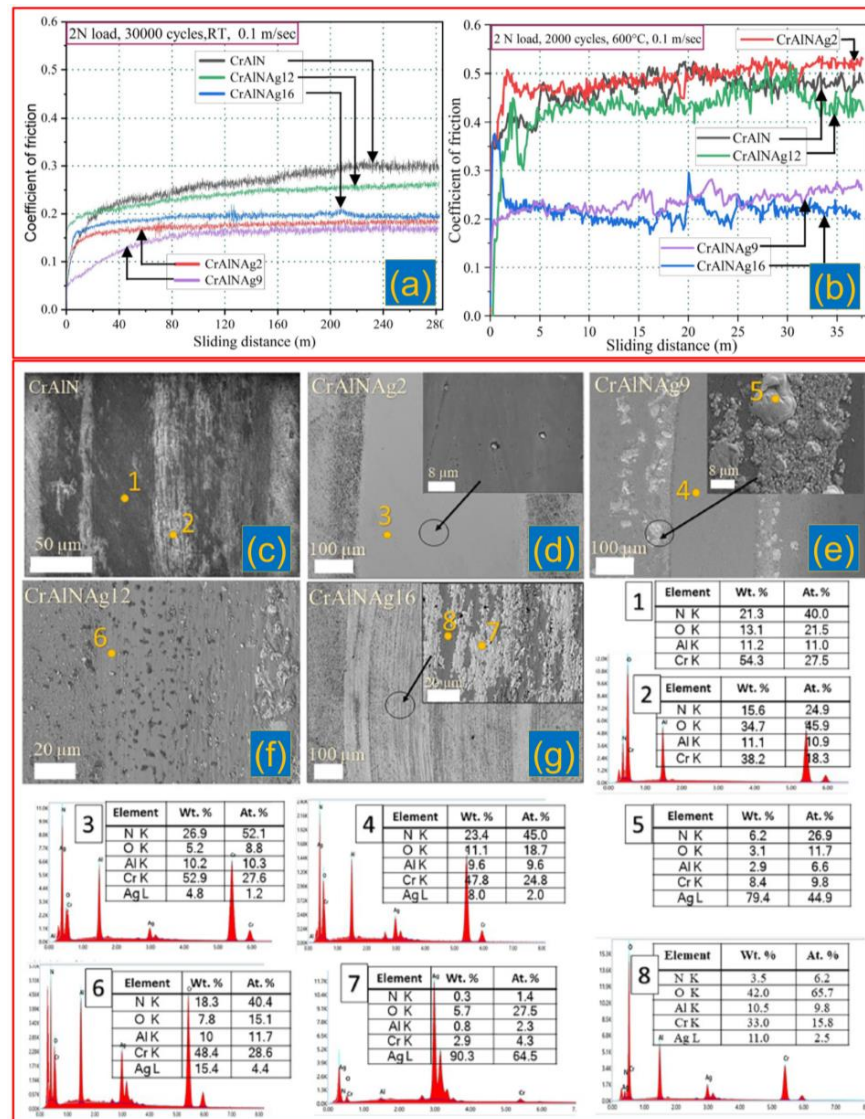


**Figure 9.** Friction, wear behavior, and tribochemical analysis of CrAlN and CrAlN(Ag) coatings. Variation in the friction coefficient of CrAlN and CrAlN(Ag) coatings tested at (a) RT and (b) 600 °C, and (c–g) wear micrographs of the bare CrAlN and CrAlN(Ag) with different Ag content coatings tested at 600 °C. The EDX spectra (1–8) represent the chemical information of wear tracks for the coatings tested at 600 °C [103]. (Reproduced with permission).

Similarly, various studies have revealed that the optimal concentration of soft/noble metals in primary ceramic hard coatings has a beneficial effect on elevated temperature applications [104–107]. Similar observations on Cu incorporated into AlTiVN coatings using HIPIMS demonstrated that the friction (0.45) and wear resistance (10–16 m<sup>3</sup>/N·m) were significantly enhanced at the optimum Cu concentration of 10.7 at% at high temperature (600 °C), as reported by Mei et al. [99]. The friction-induced oxide species, AlVO<sub>4</sub>, was primarily transferred to the lubricious Al<sub>2</sub>O<sub>3</sub>, V<sub>2</sub>O<sub>5</sub>, and CuO oxides with the addition of Cu, improving the friction and wear characteristics at elevated temperatures. On the other hand, the addition of soft metals not only improved the tribological performance of hard coatings under HT but also reduced the internal stress of the primary coatings, providing further enhancement of the desired properties. Experimental results of Ren et al. [100] on Ag incorporation into NbN coatings (Figure 10) by sputtering show a significant reduction in residual stress, which improves the coating adhesion strength, as illustrated in Figure 10a,b. The change in stress with the addition of Ag from 0–25.3 at% has a direct influence on the

friction and wear behavior of NbN-Ag coatings at different temperatures, as represented in Figure 10c,d. In HT sliding conditions, the soft metals promote the oxides, and the soft phases of these metal-rich tribolayers have self-lubricating effects. Table 2 shows a recent literature review on the properties of soft metals with hard coatings specifically for HT applications.

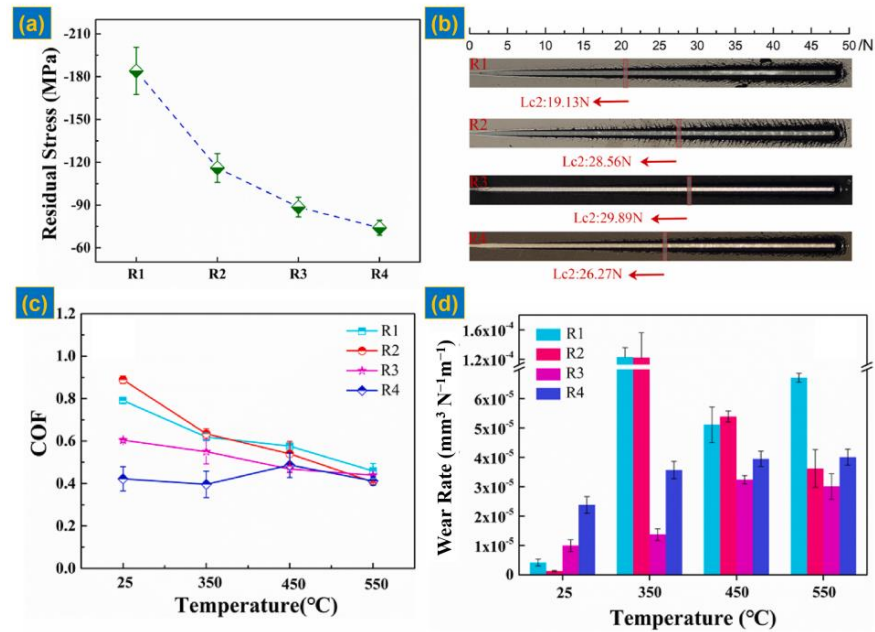


**Figure 10.** (a) Change in residual stress with the addition of Ag to NbN nanocomposite coatings at different concentrations of 0 at% (R1), 1.89 at% (R2), 15.83 at% (R3), and 25.36 at% (R4) and their corresponding (b) adhesion strength, (c) coefficient of friction, and (d) wear rates [100]. (Reproduced with permission).

**Table 2.** Recent results on Ag- and Cu-doped coatings for high-temperature tribological applications from publications in the last five years.

Coating and Dopants	Deposition Method/Post Treatments	Thickness ( $\mu\text{m}$ )	Mechanical Properties (GPa)	Tribological Properties at HT	Major Outcomes	Ref.
<b>MoN–Ag</b> (Ag: 0, 2.2, 7.9, 17.3 at%)	DC/RF magnetron sputtering	3.6–4.4	<b>H: 14.4 GPa</b> <b>E: 232 GPa</b> (for 2.2 at% of Ag)	$\mu$ : 0.27 (700 °C) <b>k: <math>2.52 \times 10^{-6} \text{ mm}^3/\text{Nm}</math></b> (for 2.2 at% of Ag)	The formation of lubricating oxides ( $\text{MoO}_3$ , $\text{Ag}_2\text{MoO}_4$ , and $\text{Ag}_2\text{Mo}_4\text{O}_{13}$ ) reduce the friction coefficient, but wear resistance decreases above 300 °C.	[108]
<b>TiSiN(Ag)</b> (Ag: 0–17 at%)	HiPIMS	2.2–2.8	<b>H: 20 GPa</b> <b>E: 218 GPa</b> (for 6 at% of Ag)	$\mu$ : 0.5 <b>k: no wear</b> (600 °C)	At 600 °C, the tribolayer consists of superficial Ag and the adhesive material from the ball counterpart to form a stable protective layer, reducing friction and causing no noticeable wear.	[104]
<b>NbN–Ag</b> (Ag: 0, 2.62, 15.83, 25.36 at%)	UBMS	1.5–3.0	<b>H: 14 GPa</b> <b>E: 261 GPa</b> (for 2.62 at% of Ag)	$\mu$ : 0.4 <b>k: <math>3.24 \times 10^{-5} \text{ mm}^3/\text{Nm}</math></b> (for 15.83 at% (Ag) at 550 °C)	The reduction in friction and the wear rate at 550 °C for the Ag (15.83 at%) sample is due to the formation of tribo-induced compacted glaze tribolayer, which is primarily composed of $\text{Nb}_2\text{O}_5$ and $\text{AgNbO}_3$ .	[100]
<b>Al–Ti–V–Cu–N</b> (Cu: 6.2, 8.0, 10.2, 10.7 and 11.7 at%)	HiPIMS	1.1–1.5	<b>H: 35.2 GPa</b> (for 6.2 at% of Cu)	$\mu$ : 0.45 (600 °C) <b>k: <math>10^{-16} \text{ m}^3/\text{Nm}</math></b> (600 °C)	The formation of predominant $\text{V}_2\text{O}_5$ and CuO lubricating oxide phases on worn surfaces results in low friction and wear at 600 °C.	[99]
<b>Mo(Cu)N</b> (Cu: 0, 5.5, 7.5, 17.8 and 24.3 at%)	Magnetron Sputtering	1.5	<b>H: 25 GPa</b> <b>E: 359 GPa</b> (for 5.5 at% of Cu, i.e., 9.2% of Cu/(Cu and Mo)) <b>H: 15.2 GPa</b> <b>E: 216 GPa</b> (for 11 at% of Ag and Cu)	$\mu$ : 0.4 <b>k: <math>3.5 \times 10^{-5} \text{ mm}^3/\text{N m}</math></b> (800 °C)	The formation of strong oxide phases, $\text{CuMoO}_4$ and $\text{MoO}_3$ , at 600 °C results in low friction and wear resistance, whereas CuO predominated at 200 °C.	[106]
<b>TiAlN (Ag, Cu)</b> (Ag and Cu: 0, 11, 16, 17 and 20 at%)	Magnetron Sputtering	2.0	<b>H: 6.7 GPa</b> <b>E: 140 GPa</b> (for 20 at% of Ag and Cu)	$\mu$ : 0.25 <b>k: <math>7.7 \times 10^{-5} \text{ mm}^3/\text{N m}</math></b> (for 17 at% of Ag and Cu)	Friction and wear reduction were due to the solid lubrication effect of out-diffused Au–Cu nanoparticles up to 17 at% in TiAlN coatings	[102]

#### 4.4. Functionally Modified Coatings

As previously discussed, the addition of Si to the CrAlN and TiAlN ternary ceramic coatings improves their high-temperature stability and wear and corrosion resistance properties. In the most promising structures of CrAlSiN and TiAlSiN coatings, a small amount of Si is used to substitute Cr/Ti atoms, causing lattice distortion due to the different atomic sizes. Additionally, the amorphous  $\text{Si}_3\text{N}_4$  matrix structure surrounding the crystalline phases regulates the grain growth, resulting in the superhard properties of these coatings. However, these solid solution and amorphous matrix structures increase the residual stress and brittle behavior of the coatings, leading to delamination of the coatings from substrates. To address these issues, coating structures are modified to finetune the microstructure to functionalize the coatings from the surface towards the substrate using gradient composition coatings. The elimination of sharp interfaces in the gradient coatings is extremely beneficial for reducing the internal stress of the coatings and improving the adhesion strength and wear resistance. According to Lu et al. [109], the adhesion strength and cutting properties of magnetron-sputtered TiAlSiN coatings were superior due to the newly fabricated out-of-plane gradient distribution of Si in the coatings. In this gradient structure, the Si content was higher on the TiAlSiN coating surface and decreases towards the substrate, effectively reducing the internal coating stress.

It can be clearly presumed that oxidation and tribolayer formation are the most crucial factors in determining the mechanical and tribological properties of hard coatings. Almost all of the literature shows that abrasive wear of sliding surfaces occurs during the initial stage and that oxidation of wear particles and coating/sliding counterbodies occurs in the majority of the samples tested under HT conditions. Depending on the temperature and nature of oxidative elements present in the coatings, the metal oxide tribolayer is the critical governing factor of friction and wear behavior. Therefore, before studying tribological

experiments, some studies have performed pre-oxidation treatments of hard coatings at elevated temperatures in an air atmosphere. In these treatments, the oxygen species will diffuse on the coatings and form oxidized surface layers to a certain depth.

For example, Lim et al. [110] conducted a comparative analysis of AlSiTiN, CrAlTiN, and CrAlSiTiN coatings with oxidized coatings annealed at 800 and 900 °C in an air atmosphere. Interestingly, the oxidized samples had lower friction and wear rates due to the formation of lubricious SiO<sub>2</sub> layers on the surface, which provided better protection against friction and wear. The machining performance of oxidized coated tools was improved due to the high presence of protective SiO<sub>2</sub> against flank wear. Surface oxides with improved hardness and low friction are formed on the sliding interfaces of Cr-, Al-, Ti-, and Si-based hard coatings during post-deposition annealing processes. As a result, coatings with surface oxide layers can easily form smooth and dense adhesive layers, potentially reducing friction and wear [111]. Other remarkable functional coating concepts from recent studies to enhance tribological performance have been achieved by designing compositionally gradient coatings [109,112–114], novel multilayer coatings [73,75,89,115, 116], and nanocomposite coatings [60].

#### 4.5. High Entropy Alloy-Based Nitride Coatings

High entropy alloys (HEAs) are the most recently developed multimetalllic alloys, in which five or more metallic elements are mixed with equal atomic ratios for the structural components in extremely high temperature and corrosive environments. The alloying elements are mixed to form a single-phase alloy based on the requirements. For instance, Chen et al. [117] reported the study of AlCrNiTiV amorphous coatings fabricated using the FCVA technique and their oxidation at 400–800 °C. The coatings annealed at 600 °C demonstrated higher hardness (22.6 GPa) and lower friction coefficients (0.22) (Figure 11a) and wear rates ( $1.1 \times 10^{-5}$  mm<sup>3</sup>/Nm) in the tribological test performed at 600 °C. The 800 °C annealed samples have extremely high oxide contents, such as Al<sub>2</sub>O<sub>3</sub>, NiCr<sub>2</sub>O<sub>4</sub>, and Cr<sub>2</sub>O<sub>3</sub>, which protect the coatings from further oxidation; however, the sudden decrease in mechanical properties results in poor tribological performance, as shown in Figure 11a. On the other hand, nitrides of these HEAs have recently been developed and their superior hardness and high-temperature stability have been demonstrated, making them suitable for harsh environmental applications. Recently, Li et al. [118] investigated the effect of nitrogen content on the mechanical and tribological properties of (MoSiTiVZr)N<sub>x</sub>, using a confocal magnetron sputtering technique with varying N<sub>2</sub> flow rates. Remarkably, a superhardness of 45.6 GPa, an elastic modulus 408 GPa, and low friction (~0.3) (Figure 11b) were attained for the N concentration of approximately 53.7 at%. The wear micrographs also show that this coating has wear resistance due to its enhanced resistance to plastic deformation with almost 50% N content present in the coating.

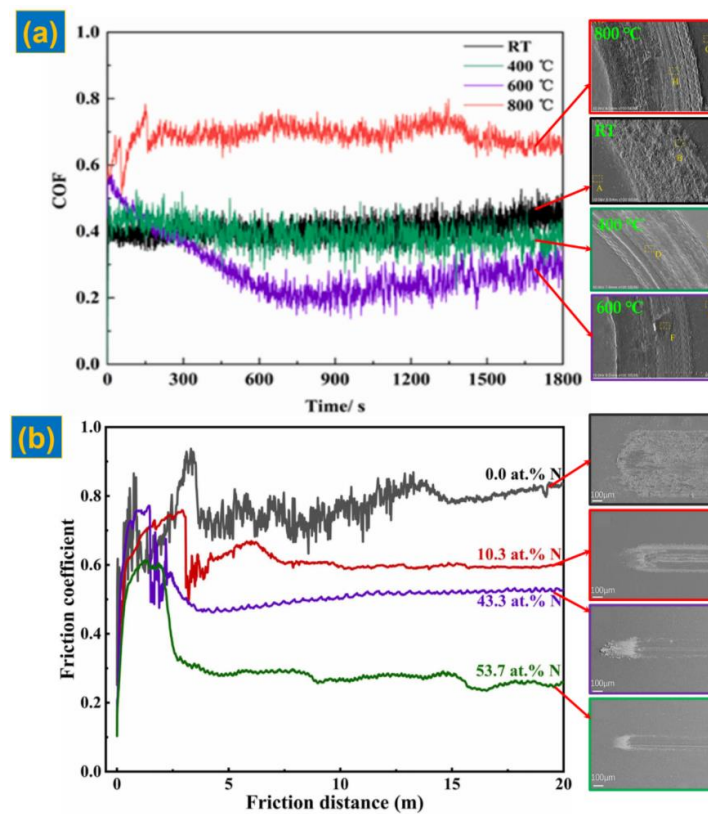


**Figure 11.** Tribological properties of HEA-based nitride coatings: (a) friction curves of AlCrNiTiV amorphous HEA coatings annealed at different temperatures (400–800 °C) tested from RT to 800 °C [117] and (b) (MoSiTiVZr) $N_x$  coatings deposited using DC sputtering with varying  $N_2$  contents of 0, 10.3, 43.3, and 53.7 at% [118]. (Corresponding wear morphologies of the HEA coatings with respect to change in temperature and N content). (Reproduced with permission).

Similar enhancements in wear as well as corrosion resistance properties were observed for other HEA nitride coatings, such as (AlCrMoSiTi) $N_x$  deposited using FVCA [119], TiZrNbTaFeN deposited using HiPIMS [120], (AlCrTiZrHf)N deposited using reactive magnetron sputtering [121], and AlCrMoZrTi/(AlCrMoZrTi)N multilayer coatings deposited using RF magnetron sputtering techniques [122]. Similar to other ceramic coatings, the residual stress plays a critical role in the mechanical and tribological properties of HEA nitride coatings, and many reports have demonstrated the optimization of substrate bias to reduce the residual stress. Lo et al. [123] investigated the effect of substrate bias on the fabrication of (AlCrNbSiTiMo)N using RF magnetron sputtering; the results revealed that the coating deposited with a (−100 V) substrate bias exhibited a higher hardness of 34.5 GPa and the lowest wear rate of approximately  $1.2 \times 10^{-6} \text{ mm}^3/\text{Nm}$  at 700 °C. Furthermore, the presence of the MoO<sub>3</sub> Magnéli phase with the addition of Mo in these HEA nitride coatings also benefits lubrication under HT sliding conditions. The higher the substrate bias, the denser the structure and smoother the coatings, which improves the wear resistance of HEA nitride coatings [124].

## 5. Failure Mechanisms of Hard Ceramic Coatings Tested under HT Sliding Conditions

The friction and wear behavior of hard coatings are primarily related to the physical, chemical, and mechanical properties at RT and elevated temperatures. Surface roughness and composition also play important roles in friction, wear debris formation, and coating deformations during initial sliding contacts. As shown in Figure 12a, asperities from both contacting surfaces interact with each other, determining the initial frictions [125]. When the friction energy is exceeded during continuous sliding motions, wear of one or both of the surfaces occurs, followed by a change in friction behavior. Depending on the nature

of the wear particles, the friction decreases when the wear particles are lubricated, and friction increases when the wear particles have difficulty producing scratches. Coatings are plastically deformed as a result of continuous sliding interactions, as locally generated frictional heat decreases the mechanical properties and accelerates the loose wear particles, resulting in coating material loss. Therefore, one of the most important criteria for harsh environmental wear protection is the selection of ceramic coatings with smoother surfaces.

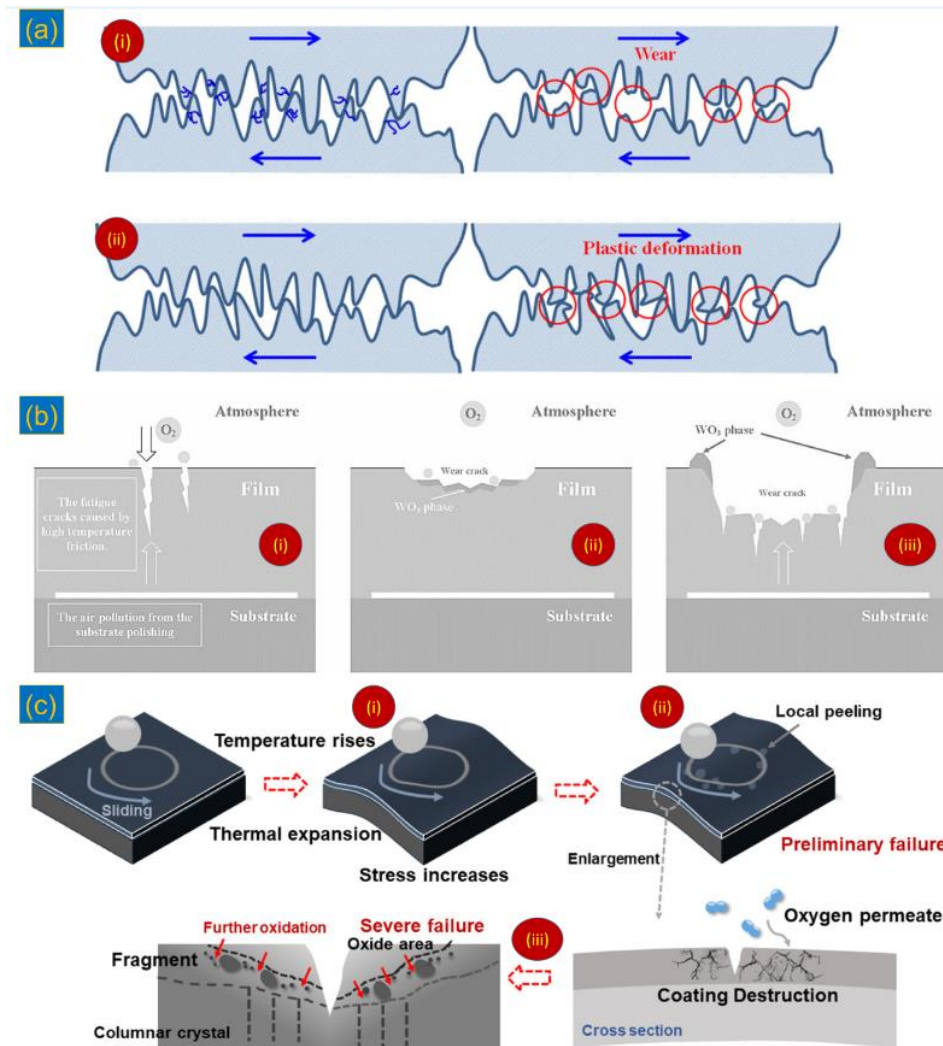


**Figure 12.** Different wear mechanisms of coatings under elevated temperature conditions. (a) Schematic of wear and deformation mechanisms [125], (b) cracking and oxidation of  $\text{Hf}_{1-x}\text{W}_x\text{N}$  coatings during high-temperature tribological experiments [93], (c) wear mechanism of TiSiN coatings tested at elevated temperature [126]. (Reproduced with permission).

Oxidation is the most unavoidable factor in determining the friction and wear mechanism of the coatings, especially at elevated temperatures. The formation of cracks during tribological interactions promotes oxidation at high temperatures. To represent the oxidation behavior, Yu et al. [93] illustrated a schematic of the oxidation process of  $\text{Hf}_{1-x}\text{W}_x\text{N}$  coatings with different W contents, as shown in Figure 12b. The crack initiated and developed at lower W ( $x = 0.37$ ) content coatings at  $600\text{ }^\circ\text{C}$ , due to the lower fracture toughness. Therefore, the atmospheric oxides enter through the crack regions and predominantly cause oxidation across the coating. Higher W additions ( $x = 0.73$ ) promote higher fracture toughness as well as  $\text{WO}_3$  lubricating oxides, resulting in a lower friction coefficient and improved wear resistance at elevated temperatures (up to  $600\text{ }^\circ\text{C}$ ). With the addition of

W ( $x = 1.0$ ), the coating became severely oxidized and the surface became more brittle, resulting in oxidative wear and deformation.

On the other hand, oxidation of coatings at high temperatures is more common in columnar structured coatings, which degrades the coating composition and causes total coating wear failure. Figure 12c depicts a schematic representation of the wear life failure mechanism of columnar coatings. Generally, three steps of failure mechanisms are involved for such columnar coatings: (i) First, thermal expansion of the coating and substrate occurs with increasing temperature (stage 1, Figure 12c(i)). (ii) Second, higher contact stress at HT conditions damage the surface and create cracks and fragments in the coating, allowing oxygen to easily penetrate and form unstable and shapeless oxides (stage 2, Figure 12c(ii)). (iii) Finally, oxygen atoms easily propagate through the columnar grains, and the wear continues with further sliding, resulting in total wear loss of the coating (stage 3, Figure 12c(iii)) [126]. Therefore, highly dense microstructures would be greatly advantageous for HT tribological applications; such coatings can be designed using novel coating structures such as nanocomposite, multicomponent, and multilayer coatings.

#### *Tribochemical Layer Formation and Failure Mechanisms of Coatings under HT Conditions*

Most of the research articles used in this present review demonstrate that the friction and wear behavior of hard coatings under RT to elevated temperatures is highly dependent on the nature of the tribolayer. Figure 13 depicts the tribological mechanism and formation of tribolayers in various nanocomposite coatings tested at RT and elevated temperatures. Figure 13a represents the variation in tribolayer formations of CrMoSiCN/Ag nanocomposite coatings with respect to Ag content (0.83, 1.64, and 2.51 at%). At lower Ag concentrations, the tribolayer, composed primarily of SiO<sub>2</sub>, transfers wear debris from Si<sub>3</sub>N<sub>4</sub> balls, as well as the oxide tribochemical species Cr<sub>2</sub>O<sub>3</sub> and MoO<sub>3</sub> from the coating surface (Figure 13a(i)). With increasing Ag, the tribolayer consists of mild SiO<sub>2</sub> from the ball, Cr<sub>2</sub>O<sub>3</sub> and MoO<sub>3</sub> oxide species from the coating, and a small fraction of Ag nanoparticles that are subjected to abrasive wear (Figure 13a(ii)). At higher Ag concentrations, a tribolayer composed of enriched Ag lubricating layers with Cr<sub>2</sub>O<sub>3</sub>, MoO<sub>3</sub>, and Ag<sub>2</sub>MoO<sub>4</sub> species, as well as transfer on the ball surface, results in combined tribochemical and abrasive wear behavior, as illustrated in Figure 13a(iii) [101].

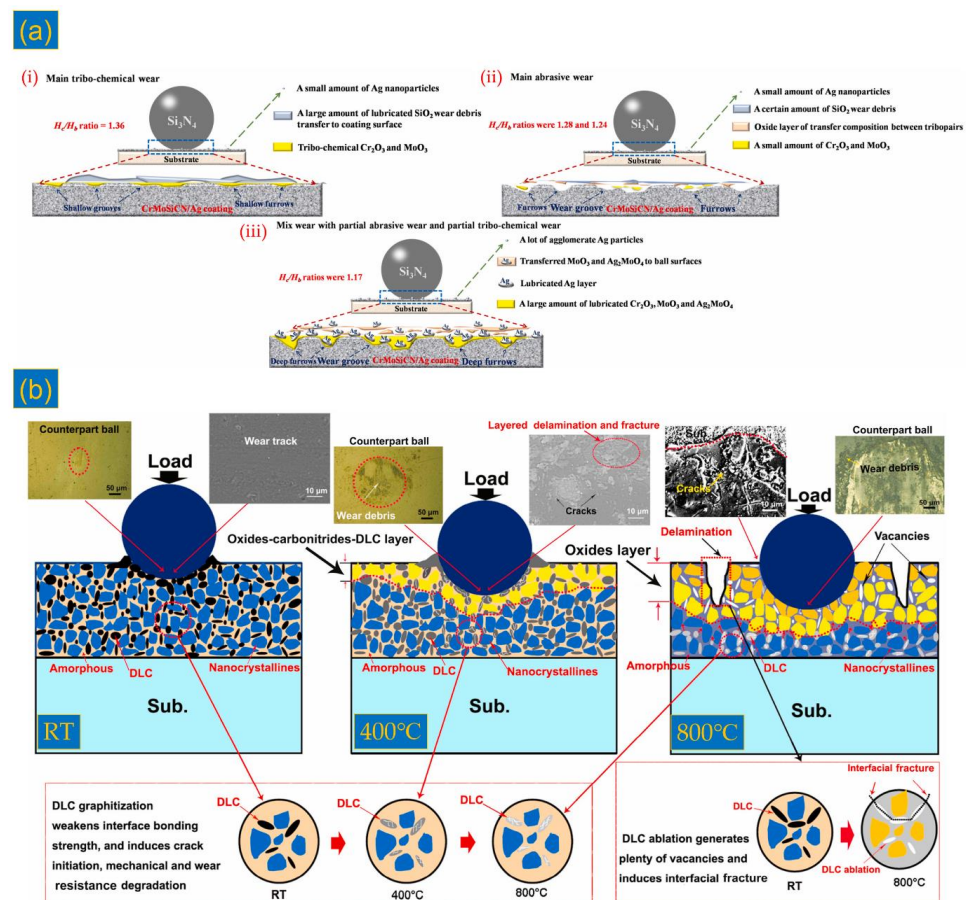


**Figure 13.** Schematic of different tribological mechanisms of nanocomposite coatings and the role of the tribolayer at RT and HT in an air atmosphere. (a) RT tribological behavior of nanocomposite Cr-MoSiCN/Ag coatings with different Ag contents: (1) 0.83 at%, (2) 1.64 at%, and (3) 2.51 at% [103] and (b) wear mechanisms of TiAlSiCN coatings at RT and elevated temperatures (400 and 800 °C) [127]. (Reproduced with permission).

Changes in the wear behavior of nanocomposite coatings and their tribological mechanisms have been discussed by Guo et al. [127] for TiAlSiCN coatings tested at RT–800 °C. The coatings are composed of nanocrystalline (Ti,Al)(C,N), diamond-like carbon (DLC), and amorphous  $\text{Si}_3\text{N}_4/\text{SiC}$  phases. Under RT conditions, the segregation of DLC at the sliding interfaces resulted in low friction and wear resistance; however, at 400 °C, the segregated DLC species started to graphitize, and carbonitride formation in the tribolayer began to deteriorate the coating fracture toughness. Extremely high graphitization and oxidative damage of coatings tested at 800 °C resulted in the severe interfacial fracture of coatings and further increased oxidation, resulting in reduced wear resistance. It can be demonstrated that carbon-rich coatings are beneficial under RT conditions, but excessive graphitization degrades the mechanical properties. Wang et al. [70] reported a similar trend in oxide forms on (Cr, V)N coatings at intermediate temperatures. Up to 600 °C, the coatings showed low friction and enhanced wear resistance properties, at 700–800 °C, the wear rate increased progressively with increased oxidation, and at 900 °C, coating breakdown due to high oxidative wear was observed.

## 6. Conclusions

In the search for hard, wear-resistant coatings for HT tribological applications, numerous research articles are published every day by researchers from all over the world. Many advanced PVD techniques have been used to create cutting-edge coating architectures with improved microstructures, grain refinement, hardness, and toughness, and their HT wear

and oxidation properties for load-bearing applications have been tested. This review examined the most recent published research articles on state-of-the-art coating architectures and their HT tribological properties. HiPIMS, FVCA, and their hybrid deposition techniques have been most recently used for the deposition of hard coatings through optimization of power, substrate bias, temperature, and partial pressure in their respective methods. Reactive as well as co-deposition methods are promising routes for these PVD methods for fabricating novel multicomponent, nanocomposite, multilayer, and gradient coatings in current research. Highlights of the innovations in recent findings are summarized below with future research aspects.

- Appropriate addition of Si and B to the TiAlN and CrAlN coatings promotes the formation of a lubricating layer consisting of SiO<sub>2</sub> and B<sub>2</sub>O<sub>3</sub>/B(OH)<sub>3</sub>, which provides lower friction and wear resistance at 800–900 °C. The a-Si<sub>3</sub>N<sub>4</sub> and a-BN<sub>x</sub> matrices around the ceramic nanocrystallites strengthen the coatings due to grain refinement. A similar effect was observed for Mo and V addition due to the formation of Mo-O and V-O Magnéli phase oxides in the tribolayer at HT (>700 °C);
- Multilayer coatings of binary, ternary, and quaternary nitride layers with nanoscale bilayer thickness exhibit remarkably high hardness (>30 GPa) and wear resistance under HT conditions. The combined protective surface oxide formation and multilayer structure restrict crack propagation, and further oxidation results in enhanced wear resistance;
- Gradient coatings with Si-rich surface layers of hard coatings demonstrate improved lubrication and ceramic nitride mechanical strength towards the substrate. Pre-oxidation of nitride coatings also favors lubricity; however, excessive oxidation deteriorates the mechanical properties;
- Appropriate soft metal (Ag and Cu) additions exhibit interesting low friction and wear resistance behavior at intermediate temperatures (up to 500 °C) due to the formation of an out-diffused Ag- and Cu-rich tribolayer;
- At very high temperatures, various coating failure mechanisms are related to the coating microstructure, compactness, and resistance to HT deformations, as well as excessive oxidation.

**Author Contributions:** Conceptualization, D.K.D. and K.K.A.M.; methodology, D.K.D. and B.R.; validation, B.R. and K.K.A.M.; resources, D.K.D.; data curation, B.R.; writing—original draft preparation, D.K.D. and B.R.; writing—review and editing, K.K.A.M.; supervision, D.K.D.; funding acquisition, D.K.D. All authors have read and agreed to the published version of the manuscript.

**Funding:** D.K.D. acknowledges the Department of Science and Technology-Science and Engineering Research Board (DST-SERB), Government of India, for a sponsored project under the Core Research Grant Scheme (Sanction order number: CRG/2018/001448). This work was also created in the frame of the project Centre for Functional and Surface Functionalized Glass (CEGLASS), ITMS code is 313011R453, operational program Research and innovation, co-funded from the European Regional Development Fund (K.K.A.M.).

**Institutional Review Board Statement:** Not applicable.

**Informed Consent Statement:** Not applicable.

**Data Availability Statement:** Not applicable.

**Acknowledgments:** The authors thank the management at Sathyabama Institute of Science and Technology, Chennai.

**Conflicts of Interest:** The authors declare no conflict of interest.

## References

1. Fox-Rabinovich, G.S.; Yamamoto, K.; Beake, B.D.; Gershman, I.S.; Kovalev, A.I.; Veldhuis, S.C.; Aguirre, M.H.; Dosbaeva, G.; Endrino, J.L. Hierarchical Adaptive Nanostructured PVD Coatings for Extreme Tribological Applications: The Quest for Nonequilibrium States and Emergent Behavior. *Sci. Technol. Adv. Mater.* **2012**, *13*, 043001. [[CrossRef](#)] [[PubMed](#)]

2. Kuo, C.-C.; Lin, Y.-T.; Chan, A.; Chang, J.-T. High Temperature Wear Behavior of Titanium Nitride Coating Deposited Using High Power Impulse Magnetron Sputtering. *Coatings* **2019**, *9*, 555. [[CrossRef](#)]
3. Ul-Hamid, A. Deposition, Microstructure and Nanoindentation of Multilayer Zr Nitride and Carbonitride Nanostructured Coatings. *Sci. Rep.* **2022**, *12*, 5591. [[CrossRef](#)] [[PubMed](#)]
4. Aissani, L.; Alhussein, A.; Zia, A.W.; Mamba, G.; Rtimi, S. Magnetron Sputtering of Transition Metal Nitride Thin Films for Environmental Remediation. *Coatings* **2022**, *12*, 1746. [[CrossRef](#)]
5. Kirnbauer, A.; Kretschmer, A.; Koller, C.M.; Wojcik, T.; Paneta, V.; Hans, M.; Schneider, J.M.; Polcik, P.; Mayrhofer, P.H. Mechanical Properties and Thermal Stability of Reactively Sputtered Multi-Principal-Metal Hf-Ta-Ti-V-Zr Nitrides. *Surf. Coat. Technol.* **2020**, *389*, 125674. [[CrossRef](#)]
6. Mersagh Dezfuli, S.; Sabzi, M. Deposition of Self-Healing Thin Films by the Sol–Gel Method: A Review of Layer-Deposition Mechanisms and Activation of Self-Healing Mechanisms. *Appl. Phys. A Mater. Sci. Process.* **2019**, *125*, 557. [[CrossRef](#)]
7. Mersagh Dezfuli, S.; Sabzi, M. Deposition of Ceramic Nanocomposite Coatings by Electroplating Process: A Review of Layer-Deposition Mechanisms and Effective Parameters on the Formation of the Coating. *Ceram. Int.* **2019**, *45*, 21835–21842. [[CrossRef](#)]
8. Sabzi, M.; Dezfuli, S.M.; Far, S.M. Deposition of Ni-Tungsten Carbide Nanocomposite Coating by TIG welding: Characterization and Control of Microstructure and Wear/Corrosion Responses. *Ceram. Int.* **2018**, *44*, 22816–22829. [[CrossRef](#)]
9. Rapuc, A.; Simonovic, K.; Huminiuc, T.; Cavaleiro, A.; Polcar, T. Nanotribological Investigation of Sliding Properties of Transition Metal Dichalcogenide Thin Film Coatings. *ACS Appl. Mater. Interfaces* **2020**, *12*, 54191–54202. [[CrossRef](#)]
10. Kumar, D.D.; Kumar, N.; Kalaiselvam, S.; Dash, S.; Jayavel, R. Wear Resistant Super-Hard Multilayer Transition Metal-Nitride Coatings. *Surf. Interfaces* **2017**, *7*, 74–82. [[CrossRef](#)]
11. Ghailane, A.; Makha, M.; Larhlimi, H.; Alami, J. Design of Hard Coatings Deposited by HiPIMS and DcMS. *Mater. Lett.* **2020**, *280*, 128540. [[CrossRef](#)]
12. Singh, A.; Ghosh, S.; Aravindan, S. Investigation of Oxidation Behaviour of AlCrN and AlTiN Coatings Deposited by Arc Enhanced HIPIMS Technique. *Appl. Surf. Sci.* **2020**, *508*, 144812. [[CrossRef](#)]
13. Yang, J.; Fu, H.; He, Y.; Gu, Z.; Fu, Y.; Ji, J.; Zhang, Y.; Zhou, Y. Investigation on Friction and Wear Performance of Volcano-Shaped Textured PVD Coating. *Surf. Coat. Technol.* **2022**, *431*, 128044. [[CrossRef](#)]
14. Khetan, V.; Valle, N.; Duday, D.; Michotte, C.; Mitterer, C.; Delplancke-Ogletree, M.P.; Choquet, P. Temperature-Dependent Wear Mechanisms for Magnetron-Sputtered AlTiTaN Hard Coatings. *ACS Appl. Mater. Interfaces* **2014**, *6*, 15403–15411. [[CrossRef](#)] [[PubMed](#)]
15. Jang, Y.J.; Kim, J.-I.; Kim, W.-s.; Kim, D.H.; Kim, J. Thermal Stability of Si/SiC/Ta-C Composite Coatings and Improvement of Tribological Properties through High-Temperature Annealing. *Sci. Rep.* **2022**, *12*, 3536. [[CrossRef](#)] [[PubMed](#)]
16. Zhang, C.; Cao, H.; Han, D.; Qiao, S.; Guo, Y. Influence of a TiAlN Coating on the Mechanical Properties of a Heat Resistant Steel at Room Temperature and 650 C. *J. Wuhan Univ. Technol. Mater. Sci. Ed.* **2013**, *28*, 1029–1033. [[CrossRef](#)]
17. Sampath Kumar, T.; Balasivanandha Prabu, S.; Manivasagam, G.; Padmanabhan, K.A. Comparison of TiAlN, AlCrN, and AlCrN/TiAlN Coatings for Cutting-Tool Applications. *Int. J. Miner. Metall. Mater.* **2014**, *21*, 796–805. [[CrossRef](#)]
18. Khetan, V.; Valle, N.; Duday, D.; Michotte, C.; Delplancke-Ogletree, M.P.; Choquet, P. Influence of Temperature on Oxidation Mechanisms of Fiber-Textured AlTiTaN Coatings. *ACS Appl. Mater. Interfaces* **2014**, *6*, 4115–4125. [[CrossRef](#)]
19. Ul-Hamid, A. Microstructure, Properties and Applications of Zr-Carbide, Zr-Nitride and Zr-Carbonitride Coatings: A Review. *Mater. Adv.* **2020**, *1*, 1012–1037. [[CrossRef](#)]
20. Al-Asadi, M.M.; Al-Tameemi, H.A. A Review of Tribological Properties and Deposition Methods for Selected Hard Protective Coatings. *Tribol. Int.* **2022**, *176*, 107919. [[CrossRef](#)]
21. Courbon, C.; Fallqvist, M.; Hardell, J.; M'Saoubi, R.; Prakash, B. Adhesion Tendency of PVD TiAlN Coatings at Elevated Temperatures during Reciprocating Sliding against Carbon Steel. *Wear* **2015**, *330–331*, 209–222. [[CrossRef](#)]
22. Nohava, J.; Dessarzin, P.; Karvankova, P.; Morstein, M. Characterization of Tribological Behavior and Wear Mechanisms of Novel Oxynitride PVD Coatings Designed for Applications at High Temperatures. *Tribol. Int.* **2015**, *81*, 231–239. [[CrossRef](#)]
23. Luo, Y.; Ning, C.; Dong, Y.; Xiao, C.; Wang, X.; Peng, H.; Cai, Z. Impact Abrasive Wear Resistance of CrN and CrAlN Coatings. *Coatings* **2022**, *12*, 427. [[CrossRef](#)]
24. Devia, D.M.; Restrepo-Parra, E.; Arango, P.J. Comparative Study of Titanium Carbide and Nitride Coatings Grown by Cathodic Vacuum Arc Technique. *Appl. Surf. Sci.* **2011**, *258*, 1164–1174. [[CrossRef](#)]
25. Chen, L.; Paulitsch, J.; Du, Y.; Mayrhofer, P.H. Thermal Stability and Oxidation Resistance of Ti-Al-N Coatings. *Surf. Coat. Technol.* **2012**, *206*, 2954–2960. [[CrossRef](#)]
26. Beake, B.D.; Smith, J.F.; Gray, A.; Fox-Rabinovich, G.S.; Veldhuis, S.C.; Endrino, J.L. Investigating the Correlation between Nano-Impact Fracture Resistance and Hardness/Modulus Ratio from Nanoindentation at 25–500 °C and the Fracture Resistance and Lifetime of Cutting Tools with Ti1–xAlxN (x = 0.5 and 0.67) PVD Coatings in Milling Operations. *Surf. Coat. Technol.* **2007**, *201*, 4585–4593. [[CrossRef](#)]
27. Peng, J.; Su, D.; Wang, C. Combined Effect of Aluminum Content and Layer Structure on the Oxidation Performance of Ti1–xAlxN Based Coatings. *J. Mater. Sci. Technol.* **2014**, *30*, 803–807. [[CrossRef](#)]
28. He, Q.; DePaiva, J.M.; Kohlscheen, J.; Beake, B.D.; Veldhuis, S.C. Study of Wear Performance and Tribological Characterization of AlTiN PVD Coatings with Different Al/Ti Ratios during Ultra-High Speed Turning of Stainless Steel 304. *Int. J. Refract. Met. Hard Mater.* **2021**, *96*, 105488. [[CrossRef](#)]

29. Hu, C.; Xu, Y.X.; Chen, L.; Pei, F.; Zhang, L.J.; Du, Y. Structural, Mechanical and Thermal Properties of CrAlN<sub>2</sub> Coatings. *Surf. Coat. Technol.* **2018**, *349*, 894–900. [[CrossRef](#)]
30. He, Q.; DePaiva, J.M.; Kohlscheen, J.; Veldhuis, S.C. Analysis of the Performance of PVD AlTiN Coating with Five Different Al/Ti Ratios during the High-Speed Turning of Stainless Steel 304 under Dry and Wet Cooling Conditions. *Wear* **2022**, *492–493*, 204213. [[CrossRef](#)]
31. Mayrhofer, P.H.; Willmann, H.; Reiter, A.E. Structure and Phase Evolution of Cr-Al-N Coatings during Annealing. *Surf. Coat. Technol.* **2008**, *202*, 4935–4938. [[CrossRef](#)]
32. Lim, K.S.; Kim, Y.S.; Hong, S.H.; Song, G.; Kim, K.B. Influence of N<sub>2</sub> Gas Flow Ratio and Working Pressure on Amorphous Mo-Si-N Coating during Magnetron Sputtering. *Coatings* **2020**, *10*, 34. [[CrossRef](#)]
33. Chang, C.-L.; Lin, C.-Y.; Yang, F.-C.; Tang, J.-F. The Effect of Match between High Power Impulse and Bias Voltage: TiN Coating Deposited by High Power Impulse Magnetron Sputtering. *Coatings* **2021**, *11*, 822. [[CrossRef](#)]
34. Sánchez-López, J.C.; Dominguez-Meister, S.; Rojas, T.C.; Colasuonno, M.; Bazzan, M.; Patelli, A. Tribological Properties of TiC/a-C:H Nanocomposite Coatings Prepared via HiPIMS. *Appl. Surf. Sci.* **2018**, *440*, 458–466. [[CrossRef](#)]
35. Anders, A. Tutorial: Reactive High Power Impulse Magnetron Sputtering (R-HiPIMS). *J. Appl. Phys.* **2017**, *121*, 171101. [[CrossRef](#)]
36. Reinhard, C.; Ehasarian, A.P.; Hovsepian, P.E. CrN/NbN Superlattice Structured Coatings with Enhanced Corrosion Resistance Achieved by High Power Impulse Magnetron Sputtering Interface Pre-Treatment. *Thin Solid Films* **2007**, *515*, 3685–3692. [[CrossRef](#)]
37. Lakhonchai, A.; Chingsungnoen, A.; Poolcharuansin, P.; Pasaja, N.; Bunnak, P.; Suwanno, M. Comparison of the Structural and Optical Properties of Amorphous Silicon Thin Films Prepared by Direct Current, Bipolar Pulse, and High-Power Impulse Magnetron Sputtering Methods. *Thin Solid Films* **2022**, *747*, 139140. [[CrossRef](#)]
38. Grigoriev, S.; Vereschaka, A.; Uglov, V.; Milovich, F.; Cherenda, N.; Andreev, N.; Migranov, M.; Seleznev, A. Influence of Tribological Properties of Zr-ZrN-(Zr,Cr,Al)N and Zr-ZrN-(Zr,Mo,Al)N Multilayer Nanostructured Coatings on the Cutting Properties of Coated Tools during Dry Turning of Inconel 718 Alloy. *Wear* **2023**, *512–513*, 204521. [[CrossRef](#)]
39. Vereschaka, A.; Grigoriev, S.; Tabakov, V.; Migranov, M.; Sitnikov, N.; Milovich, F.; Andreev, N. Influence of the Nanostructure of Ti-TiN-(Ti,Al,Cr)N Multilayer Composite Coating on Tribological Properties and Cutting Tool Life. *Tribol. Int.* **2020**, *150*, 106388. [[CrossRef](#)]
40. Gayathri, S.; Kumar, N.; Krishnan, R.; Ravindran, T.R.; Dash, S.; Tyagi, A.K.; Sridharan, M. Influence of Cr Content on the Micro-Structural and Tribological Properties of PLD Grown Nanocomposite DLC-Cr Thin Films. *Mater. Chem. Phys.* **2015**, *167*, 194–200. [[CrossRef](#)]
41. Bonse, J.; Kirner, S.V.; Koter, R.; Pentzien, S.; Spaltmann, D.; Krüger, J. Femtosecond Laser-Induced Periodic Surface Structures on Titanium Nitride Coatings for Tribological Applications. *Appl. Surf. Sci.* **2017**, *418*, 572–579. [[CrossRef](#)]
42. Geng, D.; Li, H.; Chen, Z.; Xu, Y.X.; Wang, Q. Microstructure, Oxidation Behavior and Tribological Properties of AlCrN/Cu Coatings Deposited by a Hybrid PVD Technique. *J. Mater. Sci. Technol.* **2022**, *100*, 150–160. [[CrossRef](#)]
43. Alhafian, M.R.; Chemin, J.B.; Fleming, Y.; Bourgeois, L.; Penoy, M.; Useldinger, R.; Soldera, F.; Mücklich, F.; Choquet, P. Comparison on the Structural, Mechanical and Tribological Properties of TiAlN Coatings Deposited by HiPIMS and Cathodic Arc Evaporation. *Surf. Coat. Technol.* **2021**, *423*, 127529. [[CrossRef](#)]
44. de Castilho, B.C.N.M.; Rodrigues, A.M.; Avila, P.R.T.; Apolinario, R.C.; de Souza Nossa, T.; Walczak, M.; Fernandes, J.V.; Menezes, R.R.; de Araújo Neves, G.; Pinto, H.C. Hybrid Magnetron Sputtering of Ceramic Superlattices for Application in a next Generation of Combustion Engines. *Sci. Rep.* **2022**, *12*, 2342. [[CrossRef](#)]
45. Chang, L.-C.; Zheng, Y.-Z.; Chen, Y.-I. Mechanical Properties of Zr-Si-N Films Fabricated through HiPIMS/RFMS Co-Sputtering. *Coatings* **2018**, *8*, 263. [[CrossRef](#)]
46. de Bonis, A.; Teghil, R. Ultra-Short Pulsed Laser Deposition of Oxides, Borides and Carbides of Transition Elements. *Coatings* **2020**, *10*, 501. [[CrossRef](#)]
47. Gayathri, S.; Kumar, N.; Krishnan, R.; Ravindran, T.R.; Dash, S.; Tyagi, A.K.; Raj, B.; Sridharan, M. Tribological Properties of Pulsed Laser Deposited DLC/TM (TM=Cr, Ag, Ti and Ni) Multilayers. *Tribol. Int.* **2012**, *53*, 87–97. [[CrossRef](#)]
48. Groenen, R.; Smit, J.; Orsel, K.; Vailionis, A.; Bastiaens, B.; Huijben, M.; Boller, K.; Rijnders, G.; Koster, G. Research Update: Stoichiometry Controlled Oxide Thin Film Growth by Pulsed Laser Deposition. *APL Mater.* **2015**, *3*, 070701. [[CrossRef](#)]
49. Cao, H.; Liu, F.; Li, H.; Qi, F.; Ouyang, X.; Zhao, N.; Liao, B. High Temperature Tribological Performance and Thermal Conductivity of Thick Ti/Ti-DLC Multilayer Coatings with the Application Potential for Al Alloy Pistons. *Diam. Relat. Mater.* **2021**, *117*, 108466. [[CrossRef](#)]
50. Panjan, P.; Drnovšek, A.; Terek, P.; Miletić, A.; Čekada, M.; Panjan, M. Comparative Study of Tribological Behavior of TiN Hard Coatings Deposited by Various PVD Deposition Techniques. *Coatings* **2022**, *12*, 294. [[CrossRef](#)]
51. Hirata, Y.; Takeuchi, R.; Taniguchi, H.; Kawagoe, M.; Iwamoto, Y.; Yoshizato, M.; Akasaka, H.; Ohtake, N. Structural and Mechanical Properties of A-BCN Films Prepared by an Arc-Sputtering Hybrid Process. *Materials* **2021**, *14*, 719. [[CrossRef](#)] [[PubMed](#)]
52. Sawicki, J.; Paczkowski, T. Electrochemical Machining of Curvilinear Surfaces of Revolution: Analysis, Modelling, and Process Control. *Materials* **2022**, *15*, 7751. [[CrossRef](#)] [[PubMed](#)]
53. Li, Y.; Wang, Z.W.; Zhang, Z.H.; Shao, M.H.; Lu, J.P.; Yan, J.W.; Zhang, L.; He, Y.Y. Microstructure and Tribological Properties of Multilayered ZrCrW(C)N Coatings Fabricated by Cathodic Vacuum-Arc Deposition. *Ceram. Int.* **2022**, *48*, 36655–36669. [[CrossRef](#)]

54. Shugurov, A.R.; Kuzminov, E.D. Mechanical and Tribological Properties of Ti-Al-Ta-N/TiAl and Ti-Al-Ta-N/Ta Multilayer Coatings Deposited by DC Magnetron Sputtering. *Surf. Coat. Technol.* **2022**, *441*, 128582. [[CrossRef](#)]
55. Cao, H.; Momand, J.; Syari'ati, A.; Wen, F.; Rudolf, P.; Xiao, P.; de Hosson, J.T.M.; Pei, Y. Temperature-Adaptive Ultralubrity of a WS<sub>2</sub>/a-C Nanocomposite Coating: Performance from Room Temperature up to 500 °C. *ACS Appl. Mater. Interfaces* **2021**, *13*, 28843–28854. [[CrossRef](#)] [[PubMed](#)]
56. Vuchkov, T.; Leviandhika, V.; Cavaleiro, A. On the Tribological Performance of Magnetron Sputtered W-S-C Coatings with Conventional and Graded Composition. *Surf. Coat. Technol.* **2022**, *449*, 128929. [[CrossRef](#)]
57. Cai, Q.; Li, S.; Pu, J.; Cai, Z.; Lu, X.; Cui, Q.; Wang, L. Effect of Multicomponent Doping on the Structure and Tribological Properties of VN-Based Coatings. *J. Alloys Compd.* **2019**, *806*, 566–574. [[CrossRef](#)]
58. Grigoriev, S.; Vereschaka, A.; Milovich, F.; Sitnikov, N.; Andreev, N.; Bublikov, J.; Kutina, N. Investigation of the Properties of the Cr,Mo-(Cr,Mo,Zr,Nb)N-(Cr,Mo,Zr,Nb,Al)N Multilayer Composite Multicomponent Coating with Nanostructured Wear-Resistant Layer. *Wear* **2021**, *468–469*, 203597. [[CrossRef](#)]
59. Mondragón-Rodríguez, G.C.; Hernández-Mendoza, J.L.; Gómez-Ovalle, A.E.; González-Carmona, J.M.; Ortega-Portilla, C.; Camacho, N.; Hurtado-Macías, A.; Espinosa-Arbeláez, D.G.; Alvarado-Orozco, J.M. High-Temperature Tribology of Hf Doped c-Al<sub>0.64</sub>Ti<sub>0.36</sub>N Cathodic Arc PVD Coatings Deposited on M2 Tool Steel. *Surf. Coat. Technol.* **2021**, *422*, 127516. [[CrossRef](#)]
60. Grigoriev, S.; Vereschaka, A.; Milovich, F.; Migranov, M.; Andreev, N.; Bublikov, J.; Sitnikov, N.; Oganyan, G. Investigation of the Tribological Properties of Ti-TiN-(Ti,Al,Nb,Zr)N Composite Coating and Its Efficiency in Increasing Wear Resistance of Metal Cutting Tools. *Tribol. Int.* **2021**, *164*, 107236. [[CrossRef](#)]
61. Guan, X.; Wang, Y.; Xue, Q. Effects of Constituent Layers and Interfaces on the Mechanical and Tribological Properties of Metal (Cr, Zr)/Ceramic (CrN, ZrN) Multilayer Systems. *Appl. Surf. Sci.* **2020**, *502*, 144305. [[CrossRef](#)]
62. Frank, F.; Kainz, C.; Tkadletz, M.; Czettel, C.; Pohler, M.; Schalk, N. Microstructural and Micro-Mechanical Investigation of Cathodic Arc Evaporated ZrN/TiN Multilayer Coatings with Varying Bilayer Thickness. *Surf. Coat. Technol.* **2022**, *432*, 128070. [[CrossRef](#)]
63. Xiao, B.; Liu, J.; Liu, F.; Zhong, X.; Xiao, X.; Zhang, T.F.; Wang, Q. Effects of Microstructure Evolution on the Oxidation Behavior and High-Temperature Tribological Properties of AlCrN/TiAlSiN Multilayer Coatings. *Ceram. Int.* **2018**, *44*, 23150–23161. [[CrossRef](#)]
64. Miletić, A.; Panjan, P.; Čekada, M.; Kovačević, L.; Terek, P.; Kovač, J.; Dražič, G.; Škorić, B. Nanolayer CrAlN/TiSiN Coating Designed for Tribological Applications. *Ceram. Int.* **2021**, *47*, 2022–2033. [[CrossRef](#)]
65. Wang, R.; Li, H.Q.; Li, R.S.; Mei, H.J.; Zou, C.W.; Zhang, T.F.; Wang, Q.M.; Kim, K.H. Thermostability, Oxidation, and High-Temperature Tribological Properties of Nano-Multilayered AlCrSiN/VN Coatings. *Ceram. Int.* **2022**, *48*, 11915–11923. [[CrossRef](#)]
66. Wang, T.C.; Hsu, S.Y.; Lai, Y.T.; Tsai, S.Y.; Duh, J.G. Microstructure and High-Temperature Tribological Characteristics of Self-Lubricating TiAlSiN/VSiN Multilayer Nitride Coatings. *Mater. Chem. Phys.* **2023**, *295*, 127149. [[CrossRef](#)]
67. Mei, H.; Ding, J.C.; Yan, K.; Peng, W.; Zhao, C.; Luo, Q.; Gong, W.; Ren, F.; Wang, Q. Effects of V and Cu Codoping on the Tribological Properties and Oxidation Behavior of AlTiN Coatings. *Ceram. Int.* **2022**, *48*, 22317–22327. [[CrossRef](#)]
68. Evaristo, M.; Fernandes, F.; Cavaleiro, A. Room and High Temperature Tribological Behaviour of W-DLC Coatings Produced by DCMS and Hybrid DCMS-HiPIMS Configuration. *Coatings* **2020**, *10*, 319. [[CrossRef](#)]
69. Alamgir, A.; Bogatov, A.; Jõgiaas, T.; Viljus, M.; Raadik, T.; Kübarsepp, J.; Sergejev, F.; Lümekemann, A.; Kluson, J.; Podgursky, V. High-Temperature Oxidation Resistance and Tribological Properties of Al<sub>2</sub>O<sub>3</sub>/Ta-C Coating. *Coatings* **2022**, *12*, 547. [[CrossRef](#)]
70. Wang, C.; Xu, B.; Wang, Z.; Li, H.; Wang, L.; Chen, R.; Wang, A.; Ke, P. Tribological Mechanism of (Cr, V)N Coating in the Temperature Range of 500–900 °C. *Tribol. Int.* **2021**, *159*, 106952. [[CrossRef](#)]
71. Wang, Z.; Wang, C.; Zhang, Y.; Wang, A.; Ke, P. M-Site Solid Solution of Vanadium Enables the Promising Mechanical and High-Temperature Tribological Properties of Cr<sub>2</sub>AlC Coating. *Mater. Des.* **2022**, *222*, 111060. [[CrossRef](#)]
72. Mei, H.; Wang, R.; Zhong, X.; Dai, W.; Wang, Q. Influence of Nitrogen Partial Pressure on Microstructure and Tribological Properties of Mo-Cu-V-N Composite Coatings with High Cu Content. *Coatings* **2018**, *8*, 24. [[CrossRef](#)]
73. Song, Y.; Wang, L.; Shang, L.; Zhang, G.; Li, C. Temperature-Dependent Tribological Behavior of CrAlN/TiSiN Tool Coating Sliding against 7A09 Al Alloy and GCr15 Bearing Steel. *Tribol. Int.* **2023**, *177*, 107942. [[CrossRef](#)]
74. Yeh-Liu, L.K.; Hsu, S.Y.; Chen, P.Y.; Lee, J.W.; Duh, J.G. Improvement of CrMoN/SiN<sub>x</sub> Coatings on Mechanical and High Temperature Tribological Properties through Biomimetic Laminated Structure Design. *Surf. Coat. Technol.* **2020**, *393*, 125754. [[CrossRef](#)]
75. Alamgir, A.; Yashin, M.; Bogatov, A.; Viljus, M.; Traksmaa, R.; Sondor, J.; Lümekemann, A.; Sergejev, F.; Podgursky, V. High-Temperature Tribological Performance of Hard Multilayer TiN-AlTiN/NACo-CrN/AlCrN-AlCrOAlTiCrN Coating Deposited on WC-Co Substrate. *Coatings* **2020**, *10*, 909. [[CrossRef](#)]
76. Fan, Q.; Zhang, S.; Lin, J.; Cao, F.; Liu, Y.; Xue, R.; Wang, T. Microstructure, Mechanical and Tribological Properties of Gradient CrAlSiN Coatings Deposited by Magnetron Sputtering and Arc Ion Plating Technology. *Thin Solid Films* **2022**, *760*, 139490. [[CrossRef](#)]
77. Ferreira, R.; Carvalho, Ó.; Sobral, L.; Carvalho, S.; Silva, F. Influence of Morphology and Microstructure on the Tribological Behavior of Arc Deposited CrN Coatings for the Automotive Industry. *Surf. Coat. Technol.* **2020**, *397*, 126047. [[CrossRef](#)]
78. Yan, M.; Wang, C.; Sui, X.; Liu, J.; Lu, Y.; Hao, J.; Liu, W. Effect of Substrate Rotational Speed during Deposition on the Microstructure, Mechanical and Tribological Properties of a-C: Ta Coatings. *Ceram. Int.* **2022**. [[CrossRef](#)]

79. Wang, Z.; He, Z.; Chen, F.; Tian, C.; Valiev, U.v.; Zou, C.; Fu, D. Effects of N<sub>2</sub> Partial Pressure on Microstructure and Mechanical Properties of Cathodic Arc Deposited TiBN/TiAlSiN Nano-Multilayered Coatings. *Mater. Today Commun.* **2022**, *31*, 103436. [[CrossRef](#)]
80. Chen, J.; Guo, Q.; Li, J.; Yang, Z.; Guo, Y.; Yang, W.; Xu, D.; Yang, B. Microstructure and Tribological Properties of CrAlTiN Coating Deposited via Multi-Arc Ion Plating. *Mater. Today Commun.* **2022**, *30*, 103136. [[CrossRef](#)]
81. Akhter, R.; Zhou, Z.; Xie, Z.; Munroe, P. Influence of Substrate Bias on the Scratch, Wear and Indentation Response of TiSiN Nanocomposite Coatings. *Surf. Coat. Technol.* **2021**, *425*, 127687. [[CrossRef](#)]
82. Cao, H.S.; Liu, F.J.; hao, L.L.; Luo, W.Z.; Qi, F.G.; Lu, L.W.; Nie, Z.H.; Ouyang, X.P. Effect of Bias Voltage on Microstructure, Mechanical and Tribological Properties of TiAlN Coatings. *Trans. Nonferrous Met. Soc. China* **2022**, *32*, 3596–3609. [[CrossRef](#)]
83. Akhter, R.; Bendavid, A.; Munroe, P. Tailoring the Scratch Adhesion Strength and Wear Performance of TiNiN Nanocomposite Coatings by Optimising Substrate Bias Voltage during Cathodic Arc Evaporation. *Surf. Coat. Technol.* **2022**, *445*, 128707. [[CrossRef](#)]
84. Biswas, B.; Purandare, Y.; Khan, I.; Hovsepian, P.E. Effect of Substrate Bias Voltage on Defect Generation and Their Influence on Corrosion and Tribological Properties of HIPIMS Deposited CrN/NbN Coatings. *Surf. Coat. Technol.* **2018**, *344*, 383–393. [[CrossRef](#)]
85. Lin, Y.-W.; Chih, P.-C.; Huang, J.-H. Effect of Ti Interlayer Thickness on Mechanical Properties and Wear Resistance of TiZrN Coatings on AISI D2 Steel. *Surf. Coat. Technol.* **2020**, *394*, 125690. [[CrossRef](#)]
86. Huang, B.; Zhou, Q.; An, Q.; Zhang, E.G.; Chen, Q.; Liang, D.D.; Du, H.M.; Li, Z.M. Tribological Performance of the Gradient Composite TiAlSiN Coating with Various Friction Pairs. *Surf. Coat. Technol.* **2022**, *429*, 127945. [[CrossRef](#)]
87. Ovchinnikov, S.; Kalashnikov, M. Structure and Tribological Properties of Gradient-Layered Coatings (Ti, Al, Si, Cr, Mo, S) O, N. *Surf. Coat. Technol.* **2021**, *408*, 126807. [[CrossRef](#)]
88. Bondarev, A.; Al-Rjoub, A.; Yaqub, T.B.; Polcar, T.; Fernandes, F. TEM Study of the Oxidation Resistance and Diffusion Processes in a Multilayered TiSiN/TiN(Ag) Coating Designed for Tribological Applications. *Appl. Surf. Sci.* **2023**, *609*, 155319. [[CrossRef](#)]
89. Chang, Y.Y.; Chang, B.Y.; Chen, C.S. Effect of CrN Addition on the Mechanical and Tribological Performances of Multilayered AlTiN/CrN/ZrN Hard Coatings. *Surf. Coat. Technol.* **2022**, *433*, 128107. [[CrossRef](#)]
90. Tao, H.; Tsai, M.T.; Chen, H.W.; Huang, J.C.; Duh, J.G. Improving High-Temperature Tribological Characteristics on Nanocomposite CrAlSiN Coating by Mo Doping. *Surf. Coat. Technol.* **2018**, *349*, 752–756. [[CrossRef](#)]
91. Yi, B.; Zhou, S.; Qiu, Z.; Zeng, D.C. The Influences of Pulsed Bias Duty Cycle on Tribological Properties of Solid Lubricating TiMoCN Coatings. *Vacuum* **2020**, *180*, 109552. [[CrossRef](#)]
92. Fernandes, F.; Danek, M.; Polcar, T.; Cavaleiro, A. Tribological and Cutting Performance of TiAlCrN Films with Different Cr Contents Deposited with Multilayered Structure. *Tribol. Int.* **2018**, *119*, 345–353. [[CrossRef](#)]
93. Yu, W.; Li, H.; Li, J.; Liu, Z.; Huang, J.; Kong, J.; Wu, Q.; Shi, Y.; Zhang, G.; Xiong, D. Balance between Oxidation and Tribological Behaviors at Elevated Temperatures of Hf<sub>1-x</sub>W<sub>x</sub>N Films by Optimizing W Content. *Vacuum* **2022**, *207*, 111673. [[CrossRef](#)]
94. Chim, Y.C.; Ding, X.Z.; Zeng, X.T.; Zhang, S. Oxidation Resistance of TiN, CrN, TiAlN and CrAlN Coatings Deposited by Lateral Rotating Cathode Arc. *Thin Solid Films* **2009**, *517*, 4845–4849. [[CrossRef](#)]
95. Sánchez-López, J.C.; Contreras, A.; Domínguez-Meister, S.; García-Luis, A.; Brizuela, M. Tribological Behaviour at High Temperature of Hard CrAlN Coatings Doped with y or Zr. *Thin Solid Films* **2014**, *550*, 413–420. [[CrossRef](#)]
96. Drnovšek, A.; Rebelo de Figueiredo, M.; Vo, H.; Xia, A.; Vachhani, S.J.; Kolozsvári, S.; Hosemann, P.; Franz, R. Correlating High Temperature Mechanical and Tribological Properties of CrAlN and CrAlSiN Hard Coatings. *Surf. Coat. Technol.* **2019**, *372*, 361–368. [[CrossRef](#)]
97. Cai, F.; Wang, J.; Zhou, Q.; Xue, H.; Zheng, J.; Wang, Q.; Kim, K.H. Microstructure Evolution and High-Temperature Tribological Behavior of AlCrBN Coatings with Various B Contents. *Surf. Coat. Technol.* **2022**, *430*, 127994. [[CrossRef](#)]
98. Kiryukhantsev-Korneev, P.V.; Sytchenko, A.D.; Vorotilo, S.A.; Klechkovskaya, V.V.; Lopatin, V.Y.; Levashov, E.A. Structure, Oxidation Resistance, Mechanical, and Tribological Properties of N- and C-Doped Ta-Zr-Si-B Hard Protective Coatings Obtained by Reactive D.C. Magnetron Sputtering of TaZrSiB Ceramic Cathode. *Coatings* **2020**, *10*, 946. [[CrossRef](#)]
99. Mei, H.; Ding, J.C.; Zhao, Z.; Li, Q.; Song, J.; Li, Y.; Gong, W.; Ren, F.; Wang, Q. Effect of Cu Content on High-Temperature Tribological Properties and Oxidation Behavior of Al-Ti-V-Cu-N Coatings Deposited by HIPIMS. *Surf. Coat. Technol.* **2022**, *434*, 128130. [[CrossRef](#)]
100. Ren, Y.; Jia, J.; Cao, X.; Zhang, G.; Ding, Q. Effect of Ag Contents on the Microstructure and Tribological Behaviors of NbN–Ag Coatings at Elevated Temperatures. *Vacuum* **2022**, *204*, 111330. [[CrossRef](#)]
101. Zhang, M.; Zhou, F.; Fu, Y.; Wang, Q.; Zhou, Z. Influence of Ag Target Current on the Structure and Tribological Properties of CrMoSiCN/Ag Coatings in Air and Water. *Tribol. Int.* **2021**, *160*, 107059. [[CrossRef](#)]
102. Perea, D.; Bejarano, G. Development and Characterization of TiAlN (Ag, Cu) Nanocomposite Coatings Deposited by DC Magnetron Sputtering for Tribological Applications. *Surf. Coat. Technol.* **2020**, *381*, 125095. [[CrossRef](#)]
103. Rajput, S.S.; Gangopadhyay, S.; Yaqub, T.B.; Cavaleiro, A.; Fernandes, F. Room and High Temperature Tribological Performance of CrAlN(Ag) Coatings: The Influence of Ag Additions. *Surf. Coat. Technol.* **2022**, *450*, 129011. [[CrossRef](#)]
104. Cavaleiro, D.; Veeregowda, D.; Cavaleiro, A.; Carvalho, S.; Fernandes, F. High Temperature Tribological Behaviour of TiSiN(Ag) Films Deposited by HiPIMS in DOMS Mode. *Surf. Coat. Technol.* **2020**, *399*, 126176. [[CrossRef](#)]

105. Fenker, M.; Balzer, M.; Kellner, S.; Polcar, T.; Richter, A.; Schmidl, F.; Vitu, T. Formation of Solid Lubricants during High Temperature Tribology of Silver-Doped Molybdenum Nitride Coatings Deposited by DcMS and HIPIMS. *Coatings* **2021**, *11*, 1415. [[CrossRef](#)]
106. Liu, C.; Ju, H.; Xu, J.; Yu, L.; Zhao, Z.; Geng, Y.; Zhao, Y. Influence of Copper on the Compositions, Microstructure and Room and Elevated Temperature Tribological Properties of the Molybdenum Nitride Film. *Surf. Coat. Technol.* **2020**, *395*, 125811. [[CrossRef](#)]
107. Fu, Y.; Li, H.; Chen, J.; Guo, H.; Wang, X. Microstructure, Mechanical and Tribological Properties of Arc Ion Plating NbN-Based Nanocomposite Films. *Nanomaterials* **2022**, *12*, 3909. [[CrossRef](#)]
108. Xu, X.; Sun, J.; Su, F.; Li, Z.; Chen, Y.; Xu, Z. Microstructure and Tribological Performance of Adaptive MoN–Ag Nanocomposite Coatings with Various Ag Contents. *Wear* **2022**, *488–489*, 204170. [[CrossRef](#)]
109. Lü, W.; Li, G.; Zhou, Y.; Liu, S.; Wang, K.; Wang, Q. Effect of High Hardness and Adhesion of Gradient TiAlSiN Coating on Cutting Performance of Titanium Alloy. *J. Alloys Compd.* **2020**, *820*, 153137. [[CrossRef](#)]
110. Lim, H.P.; Jiang, Z.-T.; Gan, J.H.M.; Nayan, N.; Chee, F.P.; Soon, C.F.; Hassan, N.; Liew, W.Y.H. A Systematic Investigation of the Tribological Behaviour of Oxides Formed on AlSiTiN, CrAlTiN, and CrAlSiTiN Coatings. *Wear* **2022**, *512–513*, 204552. [[CrossRef](#)]
111. Huang, B.; Zhang, E.G.; Du, H.M.; Chen, Q.; Liang, D.D.; An, Q.; Zhou, Q. Effects of Annealing Temperature on the Microstructure, Mechanical and Tribological Properties of CrAlTiN Coatings. *Surf. Coat. Technol.* **2022**, *449*, 128887. [[CrossRef](#)]
112. Tillmann, W.; Grisales, D.; Marin Tovar, C.; Contreras, E.; Apel, D.; Nienhaus, A.; Stangier, D.; Lopes Dias, N.F. Tribological Behaviour of Low Carbon-Containing TiAlCN Coatings Deposited by Hybrid (DCMS/HiPIMS) Technique. *Tribol. Int.* **2020**, *151*, 106528. [[CrossRef](#)]
113. Zhao, Y.; Xu, F.; Xu, J.; Li, D.; Sun, S.; Gao, C.; Zhao, W.; Lang, W.; Liu, J.; Zuo, D. Effect of the Bias-Graded Increment on the Tribological and Electrochemical Corrosion Properties of DLC Films. *Diam. Relat. Mater.* **2022**, *130*, 109421. [[CrossRef](#)]
114. Abedi, M.; Abdollah-zadeh, A.; Vincenzo, A.; Bestetti, M.; Movassagh-Alanagh, F.; Damerchi, E. A Comparative Study of the Mechanical and Tribological Properties of PECVD Single Layer and Compositionally Graded TiSiCN Coatings. *Ceram. Int.* **2019**, *45*, 21200–21207. [[CrossRef](#)]
115. Chang, Y.Y.; Huang, J.W. Nanostructured AlTiSiN/CrVN/ZrN Coatings Synthesized by Cathodic Arc Deposition-Mechanical Properties and Cutting Performance. *Surf. Coat. Technol.* **2022**, *442*, 128424. [[CrossRef](#)]
116. Carabillò, A.; Sordetti, F.; Querini, M.; Magnan, M.; Azzolini, O.; Fedrizzi, L.; Lanzutti, A. Tribological Optimization of Titanium-Based PVD Multilayer Hard Coatings Deposited on Steels Used for Cold Rolling Applications. *Mater. Today Commun.* **2023**, *34*, 105043. [[CrossRef](#)]
117. Chen, S.N.; Yan, W.Q.; Liao, B.; Wu, X.Y.; Chen, L.; Ouyang, X.; Ouyang, X.P. Effect of Temperature on the Tribocorrosion and High-Temperature Tribological Behaviour of Strong Amorphization AlCrNiTiV High Entropy Alloy Film in a Multifactor Environment. *Ceram. Int.* **2022**, *49*, 6880–6890. [[CrossRef](#)]
118. Li, J.; Chen, Y.; Zhao, Y.; Shi, X.; Wang, S.; Zhang, S. Super-Hard (MoSiTiVZr)<sub>Nx</sub> High-Entropy Nitride Coatings. *J. Alloys Compd.* **2022**, *926*, 166807. [[CrossRef](#)]
119. Zhao, Y.; Chen, S.; Chen, Y.; Wu, S.; Xie, W.; Yan, W.; Wang, S.; Liao, B.; Zhang, S. Super-Hard and Anti-Corrosion (AlCrMoSiTi)<sub>Nx</sub> High Entropy Nitride Coatings by Multi-Arc Cathodic Vacuum Magnetic Filtration Deposition. *Vacuum* **2022**, *195*, 110685. [[CrossRef](#)]
120. Bachani, S.K.; Wang, C.J.; Lou, B.S.; Chang, L.C.; Lee, J.W. Fabrication of TiZrNbTaFeN High-Entropy Alloys Coatings by HiPIMS: Effect of Nitrogen Flow Rate on the Microstructural Development, Mechanical and Tribological Performance, Electrical Properties and Corrosion Characteristics. *J. Alloys Compd.* **2021**, *873*, 159605. [[CrossRef](#)]
121. Cui, P.; Li, W.; Liu, P.; Zhang, K.; Ma, F.; Chen, X.; Feng, R.; Liaw, P.K. Effects of Nitrogen Content on Microstructures and Mechanical Properties of (AlCrTiZrHf)<sub>N</sub> High-Entropy Alloy Nitride Films. *J. Alloys Compd.* **2020**, *834*, 155063. [[CrossRef](#)]
122. Ren, B.; Zhao, R.F.; Zhang, G.P.; Liu, Z.X.; Cai, B.; Jiang, A.Y. Microstructure and Properties of the AlCrMoZrTi/(AlCrMoZrTi)<sub>N</sub> Multilayer High-Entropy Nitride Ceramics Films Deposited by Reactive RF Sputtering. *Ceram. Int.* **2022**, *48*, 16901–16911. [[CrossRef](#)]
123. Lo, W.L.; Hsu, S.Y.; Lin, Y.C.; Tsai, S.Y.; Lai, Y.T.; Duh, J.G. Improvement of High Entropy Alloy Nitride Coatings (AlCrNbSiTiMo)<sub>N</sub> on Mechanical and High Temperature Tribological Properties by Tuning Substrate Bias. *Surf. Coat. Technol.* **2020**, *401*, 126247. [[CrossRef](#)]
124. Zhang, X.; Pelenovich, V.; Liu, Y.; Ke, X.; Zhang, J.; Yang, B.; Ma, G.; Li, M.; Wang, X. Effect of Bias Voltages on Microstructure and Properties of (TiVCrNbSiTaBY)<sub>N</sub> High Entropy Alloy Nitride Coatings Deposited by RF Magnetron Sputtering. *Vacuum* **2022**, *195*, 110710. [[CrossRef](#)]
125. Wang, Q.; Jin, X.; Zhou, F. Comparison of Mechanical and Tribological Properties of CrBN Coatings Modified by Ni or Cu Incorporation. *Friction* **2022**, *10*, 516–529. [[CrossRef](#)]

126. Zhu, Y.; Dong, M.; Li, J.; Wang, L. Wear Failure Mechanism of TiSiN Coating at Elevated Temperatures. *Appl. Surf. Sci.* **2019**, *487*, 349–355. [[CrossRef](#)]
127. Guo, F.; Li, K.; Huang, X.; Xie, Z.; Gong, F. Understanding the Wear Failure Mechanism of TiAlSiCN Nanocomposite Coating at Evaluated Temperatures. *Tribol. Int.* **2021**, *154*, 106716. [[CrossRef](#)]

**Disclaimer/Publisher’s Note:** The statements, opinions and data contained in all publications are solely those of the individual author(s) and contributor(s) and not of MDPI and/or the editor(s). MDPI and/or the editor(s) disclaim responsibility for any injury to people or property resulting from any ideas, methods, instructions or products referred to in the content.